Mon. Not. R. Astron. Soc. **277**, 1293–1311 (1995)

The metallicity gradient of the Galactic bulge★

Dante Minniti,[1,2]† Edward W. Olszewski,[2] James Liebert,[2] Simon D. M. White,[3] John M. Hill[2] and Michael J. Irwin[3]

[1]*European Southern Observatory, D-85748 Garching b. München, Germany*
[2]*Steward Observatory, University of Arizona, Tucson, AZ 85721, USA*
[3]*Institute of Astronomy, Madingley Road, Cambridge CB3 0HA*

Accepted 1995 July 4. Received 1995 May 19; in original form 1995 February 9

ABSTRACT

We determine metallicities for a large number of K giants at 1.5–1.7 kpc from the Galactic Centre, based on medium resolution spectra. We study the bulge metallicity gradient by comparing the present spectroscopic observations with previous metallicity determinations at Baade's window (BW), at 0.5 kpc from the Galactic Centre. It is confirmed that: (1) there is a metallicity gradient within the inner 2 kpc of the Galaxy; (2) at any given distance from the Galactic Centre, there is a large spread in metal abundances.

Key words: stars: abundances – Galaxy: evolution – Galaxy: formation.

1 INTRODUCTION

Baade (1951) discovered RR Lyrae stars in a region with a high density of stars towards the centre of the Galaxy. This region of low obscuration is now called Baade's window (BW), and it has remained as the most important, best-studied bulge field. Because of the RR Lyrae stars, Baade postulated that the bulge was old and metal-poor, like the halo globular clusters.

The relationship of the bulge, found in the central 2 kpc of the Galaxy, with the halo is not clear. Arp (1955, 1965) published a photographic *BV* colour–magnitude diagram (CMD) of BW, finding that the bulge population was globular cluster-like, showing few blue stars, a populated red giant branch and a red horizontal branch (see also van den Bergh 1971). However, Nassau & Blanco (1958), and Blanco (1965) found that the ratio of carbon to M giant stars of the bulge was almost zero, in marked contrast with the Galactic disc. This discovery challenged Baade's hypothesis of an old, metal-poor bulge.

Later, Whitford (1978) showed that the integrated spectra of bulge windows resembled those of distant elliptical galaxies and bulges. These galaxies have very strong lines which look like a metal-rich population, confirming the results presented by Morgan at the Vatican Conference (also Morgan & Mayall 1957). These results were followed up with the determination of the chemical abundance of bulge giants by Rich (1988), who found that the mean metallicity of K giants at Baade's window was [Fe/H] = +0.3. Recently, new abundances of similar stars measured by McWilliam & Rich (1994) bring down the mean metallicity of the bulge to more moderate values. They find a mean metallicity [Fe/H] = −0.25 from echelle spectra, model atmospheres and spectrum synthesis techniques. Obviously, an independent confirmation of the absolute metallicity of the Galactic bulge, by spectroscopic methods, is desirable.

The determination of existence of an abundance gradient in the central regions of the Milky Way is important for testing models of Galaxy formation. Generally speaking, there are two competing scenarios championed by Eggen, Lynden Bell & Sandage (1962, hereafter ELS), and by Searle & Zinn (1978, hereafter SZ). The ELS formation scenario was designed to explain the formation of the Galactic halo and disc, and it is essentially a dissipational collapse model. Here, progressive self-enrichment occurred as the collapse proceeded inwards, and a metallicity gradient is predicted. In such a scenario, metallicity, age and kinematics are correlated. This model was explored theoretically for example by Larson (1976) and Carlberg (1984).

SZ proposed that the halo was formed from the coalescence of smaller protogalactic fragments, during an extended period of time, in a collapse that was not homogeneous. This is reminiscent of the merger scenarios advanced by Toomre (1977). In this SZ scenario, it is not obvious that there will be a metallicity gradient. For example, mergers will mix the stellar populations and reduce the metallicity gradients

★Based on observations collected at the MMT Observatory, a joint facility of the University of Arizona and the Smithsonian Institution, and at the Cerro Tololo Inter-American Observatory, operated by the Association of Universities for Research in Astronomy, NOAO, under a co-operative agreement with the National Science Foundation.
†Visiting Astronomer, Cerro Tololo Inter-American Observatory, NOAO.

(White 1980). Indeed, one of the stronger arguments in favour of the SZ picture of halo formation is the lack of a metallicity gradient in the halo (e.g. Zinn 1985; Armandroff, DaCosta & Zinn 1992). However, the inner bulge may be different from the halo.

There are several sets of observations designed to test these models, both in external galaxies and in the Milky Way. In particular, based on optical colours, Balcells & Peletier (1994) found metallicity gradients in the bulges of a large sample of spirals, selected to minimize the dust contribution. At the same time, Balcells & Peletier (1994) found that the metallicity gradients increase as a function of bulge size, also consistent with the predictions of dissipational collapse models (e.g. Carlberg 1984).

For the Galactic bulge, recently published results differ in the extent, amplitude or even existence of such a gradient for $R \leq 2$ kpc. For example, Terndrup (1988) finds that the metallicity decreases by about 0.7 dex kpc^{-1} along the minor axis of the Galaxy. This is confirmed by Terndrup et al. (1990). On the other hand, Tyson & Rich (1993) do not find a metallicity gradient in the inner bulge, concluding that the bulge may have formed via dissipationless collapse.

An alternative model for bulge formation in late-type spirals was proposed by Pfenniger & Norman (1990, see also Sellwood 1993), who argue that a strong bar potential in the inner disc could create a concentration of stars at the centre, which are then heated out of the Galactic plane by resonances, forming the bulge. It would be natural, then, to ask if such a scenario would produce metallicity gradients in the resulting bulges. Observations of H II regions in a large number of spirals confirm that inner abundance gradients become shallower for the galaxies with the stronger bars (Martin & Roy 1994; Zaritsky et al. 1994). Interestingly, the flattening of metallicity gradients is predicted by recent numerical simulations of barred galaxies (Friedli, Benz & Kennicutt 1994). As numerous evidence now supports that the Milky Way is a barred galaxy (Blitz & Spergel 1991; Binney et al. 1991; Stanek et al. 1994; Dwek et al. 1994), it would be profitable to determine the presence and extent of a metallicity gradient in the bulge.

The specific objectives of the present report are, then, to determine the metal abundance of the Galactic bulge, and to determine if there is a metallicity gradient in the inner Galaxy. We assume that the inner Galaxy is composed of a flat, kinematically cold disc, a halo and a bulge. These components are defined in terms of their metallicities and kinematics. In particular, the inner disc and halo are assumed to be analogous to the local disc and halo, and the bulge can be described as an oblate isotropic rotator (Kent 1992). We will also assume that most of the stars are located at distances where the density along the line-of-sight reaches its maximum value for each component (following Blanco & Terndrup 1989). In this paper we present spectroscopy and derive metallicities for more than 400 bulge K giants in two different fields. We compare our results with existing bulge data at different Galactocentric distances to determine the existence and amplitude of the metallicity gradient in the bulge.

The paper is organized in the following way. Section 2 discusses the data (selection of candidates, observations and reductions). Section 3 explains the metal abundance determinations. Section 4 presents the metallicity distribution in the two fields. Section 5 discusses other possible bulge tracers such as M giants, Miras, planetary nebulae and RR Lyrae. Section 6 reviews the evidence of a metallicity gradient from photometry and spectroscopy. Section 7 addresses the absolute metallicity of the Galactic bulge. Section 8 is a summary of the present knowledge of bulge chemical evolution. Section 9 discusses the formation of the Galactic bulge. Finally, the main conclusions are summarized in Section 10.

2 THE DATA

The observations and reduction procedures are described in detail by Minniti (1993; see also Minniti et al. 1992; Minniti 1995a), here we present a brief summary.

2.1 Selection of candidates

Of the three fields observed by Minniti (1995c), we use here only the two with the highest latitudes. The other field at $(l, b) = (12°, 3°)$ is heavily contaminated by disc stars, and it will not be considered here, since we are interested in the metallicity of the bulge. We also note that the selection of giants for both fields studied here was different, which should give us an external check on the results.

The candidates in the field F588 at $(l, b) = (8°, 7°)$ were selected on the basis of *BRI* photometry (see Minniti et al. 1992). The optical colour–colour diagrams played a role in this field to discriminate the (not numerous) foreground unreddened dwarfs. Photographic photometry in the $B_j RI$ bands of plates of the UK Schmidt Telescope (UKST) survey was obtained with the APM machine by one of us (MI), using the standard APM procedure and internal calibrations. The transformation to the standard Johnson *B*, Cousins *R* and *I* systems was performed via CCD observations obtained at the 90-inch telescope of the Steward Observatory. We followed the standard CCD reduction procedures within IRAF, and the CCD photometry was obtained using DAOPHOT (Stetson 1987). Finally, we selected stars uniformly in F588 with magnitudes $R \geq 15$, and colours $B-R \geq 1.10$ and $R-I \geq 0.7$. These $B-R$ and $R-I$ colours are transformed to $B-V$ colours using the relationships given by Bessell (1986), which are independent of [Fe/H] to first order.

Cudworth (1986) presents proper motions and photographic photometry for stars in the field of the globular cluster M22 at $(l, b) = (9.9, -7.6)$. We select a suitable sample of bulge giants based on the location of stars in the colour–magnitude diagram of Cudworth (1986), and our own IR photometry. Taking into account the flattening of the bulge, the CMD in the M22 field should be similar to the CMD in the 10° field of Terndrup (1988). Allowing for the different reddenings, this expectation is confirmed by the data, as the fainter and redder stars in the CMD of Cudworth (1986) lie in the expected location of bulge red giants. Then, all the stars with $(B-V) \geq 0.8$, $V \leq 14$, and cluster membership probability smaller than 99 per cent, were included in our candidate list. We took spectra of 99 stars out of a total 101 in that sample. We also included several giant members of M22 in the spectroscopic sample as an external check. Optical IR colour–colour diagrams were checked to neglect nearby dwarfs in this field.

2.2 The spectroscopic observations

The data were collected in four observing runs: two nights in 1992 August at the CTIO 4-m telescope with the multifibre spectrograph Argus (Ingerson 1988), four nights in 1990 June/July at the Steward Observatory 90-inch telescope with the multifibre spectrograph MX (Hill & Lesser 1988), and two nights in 1991 July at the Multiple Mirror Telescope (MMT) Observatory with the Red Channel spectrograph (Schmidt, Weymann & Foltz 1989).

With the Argus at the CTIO 4-m telescope, we used the bench spectrograph with the 632-line grating KPGL1 blazed at 4200 Å. The exposure time was ~40 min, about 20 fibres produced good signal-to-noise (S/N) spectra per fibre configuration, at ~2.5-Å resolution. The spectral coverage is from 4700 to 5700 Å.

The spectra obtained at the MMT with the Red Channel spectrograph have a spectral coverage from 4600 to 5350 Å. We used the 800 × 800 TI CCD chip and an 800-line grating in second order blazed at 5000 Å, the resulting resolution being ~1.8 Å. Typical exposure times were between 20 and 30 minutes. The slit size projected on the sky is 1.5 × 180 arcsec^2. We have selected typically pairs of star candidates, and rotated the instrument to accommodate them on the slit at the same time.

MX allows automatic positioning of the fibres to obtain spectra for 32 stars at a time. We used the 800 × 800 TI CCD chip and a 1200-line grating in second order blazed at 5200 Å, obtaining a resolution of ~2 Å. The spectral coverage is from 4550 to 5400 Å. The exposure times for the programme stars ranged from 20 to 35 min.

In all these runs we observed a variety of giants in globular and open clusters that are used as metal abundance and luminosity standards (Minniti 1995a).

2.3 Data reduction

To reduce the spectra, we have followed the standard procedures within the IRAF environment, using the routines in the package CCDRED. The CCD frames were overscan and bias subtracted, and trimmed to remove the unused parts of the images. Then they were divided by a high S/N flat field (dome quartz lamp) that was previously normalized by fitting a high-order surface, leaving only the pixel to pixel response. The next steps in the reductions differ according to the instrument used, and we will describe them in turn.

The Argus reductions were done following the precepts of Suntzeff et al. (1993), as described by Minniti (1995a). The spectra were extracted in IRAF within the ARGUS package. First, the spectra for all apertures were traced with a low-order spline function using a high S/N flat field. Then, the objects, skies and comparison lamps were extracted into one-dimensional spectra. The fibres were corrected to give uniform transmission using a very high S/N sky exposure. The one-dimensional spectra were wavelength calibrated interactively and rebinned to the same dispersion and wavelength coverage. The sky subtraction was also done interactively, and locally, using a median of the four nearest sky fibres to account for local focus changes.

The reduction procedure for the MMT data were summarized in Minniti et al. (1992). The spectra were traced and extracted to one dimension using the TWODSPEC package in IRAF. First we trace the object spectra (typically 2–3 per frame) interactively with a low-order spline function. At the same time the sky subtraction was performed taking two 10-pixel-wide windows on either side of the stellar spectrum. In general, the sky subtraction was cleaner with the slit than with the fibre spectra. The spectra were wavelength calibrated and placed on a linear wavelength scale.

The MX data reduction was also described by Minniti et al. (1992). The MX spectra were extracted in IRAF with the MXPACKAGE (written by J. Hill). We traced the spectra for all apertures with a low-order spline function using a high S/N twilight exposure. That frame also defined the width of the aperture windows to include all of the starlight. Then the objects, skies and comparison lamps were extracted into one-dimensional spectra. The fibres were corrected to give uniform transmission using a very high S/N sky exposure. The one-dimensional spectra were wavelength calibrated interactively and rebinned to the same dispersion and wavelength coverage. The sky subtraction was also done interactively, deriving a median of all the sky fibres.

Finally, cosmic ray blemishes in all the spectra were interpolated interactively. We note that no extinction correction or flux calibration was attempted. However, the sky spectra were checked to see that there were not more than a few per cent continuum variations from fibre to fibre.

Owing to the nature of fibre selection algorithms, several programme stars were observed twice and a few were observed three times on different nights. These multiple observations of giants in the bulge and in well known globular clusters allowed us to make a good estimate of the true errors in the spectroscopic indices.

3 METALLICITY DETERMINATIONS

To obtain luminosity classifications and metallicity estimates, we define a set of spectrophotometric indices of line intensities following Faber et al. (1985) and Friel (1987). Each index is defined as the ratio of the average flux in the central feature passband to that of the continuum passbands located at the sides, and it is expressed in terms of magnitudes. The indices were measured in the rest frame of the star, with geocentric velocity corrections made to the passbands. This is important, because some of the stars have velocity moduli in excess of 100 km s^{-1}, which would represent a significant portion of some of the passbands used in the indices.

Given that the metallicities derived by Rich (1988) were uncertain (McWilliam & Rich 1994), it is worrisome to use similar line indices. However, we have improved the procedure by observing a large number of calibrators of known abundance, and by selecting them carefully (Minniti 1995a). We have observed many giants with known abundances in the field, in open clusters and in globular clusters (about 400 stars in total). Based on these spectra, we have constructed a grid to calibrate metallicities as function of colour, but using only the globular cluster giants. We find that the open clusters and field stars do not follow the same calibration. This is consistent with the results of Friel & Janes (1993) and of McQuitty et al. (1994), who find that the relative Mg strength with respect to Fe is different for various open clusters, and is correlated with their ages. These observations could be due to different element ratios, indicative of a different chemical evolution history (i.e. the competition

between SN II and SN I) (McQuitty et al. (1994). Gorgas et al. (1993) also pointed out a systematic – unexplained – difference between the indices of the field stars and globular cluster stars.

We circumvent the problem by using only globular clusters (Minniti 1995a). Thus, the metallicities we quote are on the globular cluster system of abundances, as compiled by Armandroff (1989). The reasons for using the globular clusters as calibrators are given by Minniti (1995d), and can be summarized as follows: (1) the initial exploration of McWilliam & Rich (1994) suggests that some element ratios in bulge giants are similar to those of globular cluster giants (e.g. Sneden et al. 1994), implying a similar chemical evolution history. (2) The few metal-rich globular clusters with measured ages seem to be as old as the bulge. (3) They form a spheroidal system, as opposed to a disc system (Frenk & White 1982).

A set of seven and five indices are measured for the Argus and MMT data, respectively. These indices are defined in Table 1: column 2 lists the central bandpasses; columns 3 and 4 show the continuum bandpasses; column 4 lists the dominant species for each index, and column 5 gives the parameter to which the indices are most sensitive (i.e. temperature, luminosity or metallicity). The indices Fe4680, Fe5335 and Fe5400 for the MMT spectra, and the index Fe4680 for the Argus spectra were not measured because they fell outwith the wavelength range covered.

The spectroscopic indices for the different instrument set-ups agree with each other, provided small zero-point offsets are applied. These shifts are: ΔMg = 0.04, ΔFe5270 = 0.00 and ΔFe5335 = 0.02, in the sense Argus minus MMT. Note that these zero-point offsets are of the order of or smaller than the scatter in the index measurements. Similar shifts were applied to the MX data (e.g. Minniti et al. 1992).

The mean errors in the spectrophotometric indices, derived from comparison of repeat observations, is computed following Pier (1983). For the MMT data, the errors in the spectral indices are σ(Mg) = 0.05, σ(Fe4680) = 0.04, σ(Fe4590) = 0.04, σ(Fe4920) = 0.04, σ(Fe5011) = 0.05, σ(Fe5270) = 0.04 and σ(Fe5335) = 0.03 for the spectra with S/N $\geq$ 5. For the Argus data, the errors in the spectral indices are σ(Mg) = 0.05, σ(Fe4680) = 0.04, σ(Fe4590) = 0.04, σ(Fe4920) = 0.04, σ(Fe5011) = 0.05, σ(Fe5270) = 0.04 and σ(Fe5335) = 0.03 for the spectra with S/N $\geq$ 8. We stress that even when the instrumental set-ups and the calibrations were different, the good agreement supported the accuracy of the data.

The final abundances will be derived using the combination of the indices Mg, Fe5270 and Fe5335, which we shall call the Mg + 2Fe index. In spite of the different behaviour of these indices, this particular combination was found to be the best, among the ones analysed for measuring metallicities (see also Faber et al. 1985; Friel 1987). We decided to use the sum, rather than calibrate each index separately, to allow metallicity determinations for the lower S/N spectra.

The metallicities are derived following the calibration given by Minniti (1995a). Our calibrating grid gives [Fe/H] for each star from its Mg + 2Fe index and $B-V$ colour. As an example, Fig. 1 shows four of our calibrating clusters, along with the grid lines. The cluster giants shown are from the metal-poor globular clusters M 3 with [Fe/H] = −1.66, from the intermediate metallicity globular cluster M 4 with [Fe/H] = −1.05, and from the metal-rich clusters 47 Tuc with [Fe/H] = −0.71 and NGC 6356 with [Fe/H] = −0.5. Apart from a few red outliers (which are M giants with strong TiO bands in all cases) and some scatter, Fig. 1 shows that the Mg + 2Fe index is a good metallicity discriminator.

The dispersion observed for the giants within a given cluster in the Mg + 2Fe versus $B-V$ diagram is larger than that due to the typical measurement errors. Thus, the dispersion observed in the index strength is intrinsic, and not entirely due to measurement errors. It was also found that

Table 1. Definition of spectral indices.

INDEX	CENTER	CONT 1	CONT 2	SPECIES	CRITERIA
Mg	5130.0-5200.0	4935.0-4975.0	5303.0-5367.0	Mgb+MgH	lum-met
Mg1	5071.0-5134.7	4897.0-4958.2	5303.0-5366.7	MgH	lum-met
Mg2	5156.0-5197.2	4987.0-4958.2	5303.0-5366.7	Mgb	lum-met
Mgb	5162.0-5193.2	5144.5-5162.0	5193.2-5207.0	Mgb	lum-met
MgH	5200.0-5212.0	4897.0-4958.2	5303.0-5366.7	MgH	lum-met
Hβ	4845.0-4875.0	4829.5-4848.2	4878.0-4892.0	H,FeI	temp
Fe4680	4636.0-4723.0	4606.0-4636.0	4736.0-4773.0	FeI,CrI,NiI,MgI	met
Fe4920	4900.0-4940.0	4796.0-4841.0	4935.0-4975.0	FeI	met
Fe4980	4975.0-4989.0	4935.0-4975.0	5051.0-5096.0	FeI	met
Fe5011	4976.0-5051.0	4935.0-4975.0	5051.0-5096.0	FeI,FeII,NiI,TiI	met
Fe5270	5248.0-5287.0	5220.0-5250.0	5288.0-5322.0	FeI,CaI	met
Fe5335	5315.0-5353.0	5308.0-5317.0	5356.0-5460.0	FeI,CrI	met
Fe5400	5384.0-5430.0	5356.0-5364.7	5430.0-5460.0	FeI	met

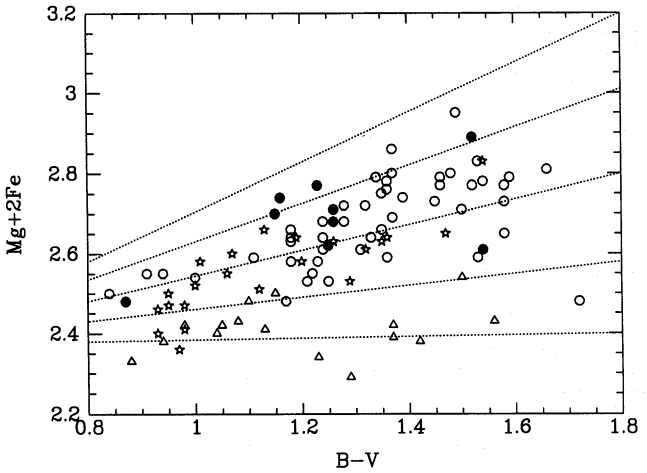

Figure 1. Mg + 2Fe index versus dereddened $B-V$ colour for globular cluster giants of well-known abundances. The cluster giants shown here are from M 3 with [Fe/H] = −1.66 (triangles), M 4 with [Fe/H] = −1.05 (stars), 47 Tuc with [Fe/H] = −0.71 (open circles) and NGC 6356 with [Fe/H] = −0.5. The dotted lines correspond to our grid of isoabundances (Minniti 1995a), with [Fe/H] = −1.75, −1.5, −1.0, −0.5 and 0.0, from bottom to top.

the errors in the metallicities were dependent on metal abundance, in the sense that the scatter is larger for the more metal-rich clusters. This is contrary to the expectations, since the spectral features are much weaker in the more metal-poor spectra.

The indices measured for all the stars in the F588 and M22 fields are listed in Tables 2 and 3, respectively. The indices for 36 M giants in the same are given for completeness, these interlopers are not considered in the rest of the paper. Figs 2(a) and (b) present the combined Magnesium and Iron index versus colour, corrected for reddening for both fields. The isoabundance lines from the calibration are also shown. Fig. 2(b) shows that the M22 giants (filled circles) are indeed metal-poor; they were used to check the metal-poor end of the calibration.

Tables 4 and 5 lists magnitudes, colours and final abundances for the giants in both fields.

4 BULGE METALLICITY DISTRIBUTION

The metallicity distribution for the observed giants with $R \geq 13.5$ in F588 is given in Fig. 3(a). There is a wide range of metal abundances in the field. There are very metal-poor halo stars, as well as very metal-rich bulge giants. Note that the scatter in the metallicity determinations increases for the most metal-rich giants, as discussed above. This would artificially widen the metallicity distributions at the metal-rich end. Fig. 4 shows a Lucy deconvolution of the observed distribution, in an attempt to take into account the errors, since we know the dependence of the errors as a function of metallicity from the observations of giants in globular clusters. The metallicity errors are $\sigma_{[Fe/H]} = 0.15$ for [Fe/H] ≤ −1.0, and $\sigma_{[Fe/H]} = 0.10[Fe/H] + 0.25$ for [Fe/H] ≥ −1.0. Fig. 4, therefore, is a better representation of the real metallicity distribution of field F588. We can see from this estimate of the 'true' metallicity distribution in field F588 that the mean abundance is less than solar, and that there is still a large range of metallicities, [Fe/H] from −2 to about +0.5.

The fact that the errors increase for the more metal-rich stars to $\sigma_{[Fe/H]} = 0.4$ casts doubts on the reality of the values for the most metal-rich stars. Indeed, it is not clear whether there are any stars in our sample with [Fe/H] ≥ +0.5. It should be pointed out that for field F588, we selected the stars uniformly over the whole range occupied by bulge K giants in the colour–colour and colour–magnitude diagrams. We note that the same selection effect holds for the sample of Rich (1988) in Baade's window. The reddening in this field is found to be homogeneous, so that the metallicities are not affected by differential reddening.

The kinematic evidence suggests that most of the stars that are more metal-poor than [Fe/H] = −1 belong to the inner extension of the halo rather than to the bulge itself (Minniti 1995c). This is also the natural 'break' in [Fe/H] between halo and thick disc in the solar neighbourhood (e.g. Carney, Latham & Laird 1990; Norris, Bessell & Pickles 1985). Excluding possible halo stars (with [Fe/H] ≤ −1), the mean metallicity of the 'pure' bulge giants observed in field F588 would be [Fe/H] = −0.3. This mean abundance could be ~0.15 dex lower if we have seriously overestimated the metallicity of the most metal-rich giants.

Fig. 3(b) shows the metallicity distribution for the bulge giants with $V \geq 14.0$ in the field of M22. The brighter stars may be disc members. The field of the globular cluster M22 also appears to be relatively uniform in terms of extinction. As discussed by Minniti, Coyne & Claria (1992), the SE part of the M22 field is only slightly more reddened. This differential reddening will not affect the metallicities determined here. The observed bulge giants show a mean abundance of [Fe/H] = −0.65, but a wide range of metallicities is present, arising only in part from our measurement errors (see errorbars in Fig. 3a). The mean metallicity and metallicity distribution in the M22 field are in excellent agreement with those of the F588 field, even though the criteria applied to select the bulge giants was different for both fields. The only difference between both distributions is that the proportion of metal-poor stars (with [Fe/H] ≤ −1.0) is slightly larger in the M22 field than in F588. In the M22 field, we find that 22 K giants have [Fe/H] ≤ −1.0, versus 52 K giants with [Fe/H] ≥ −1.0. This is due to our selection of stars in the Cudworth (1986) sample, we are biased towards picking metal-poor giants. Therefore, Fig. 3(b) may not represent the real metallicity distribution of this field; it could be incomplete for the metal-rich end.

Fig. 5 shows the observed metallicity distribution in fields F588 (at $R = 1.5$ kpc) and M22 (at $R = 1.6$ kpc), compared with that re-scaled by Rich (1988), following McWilliam & Rich (1994) for Baade's window (at $R = 0.5$ kpc), and with that of Morrison & Harding (1993) in a field at $(l, b) = (-10°, -10°)$. Already two of our major conclusions can be inferred from this figure: (1) there is a metallicity gradient within the inner 2 kpc of the Galaxy. (2) At any given distance from the Galactic Centre there is a large spread in metal abundances. Part of this spread is caused by the metallicity gradient combined with the line-of-sight depth expected in any bulge sample.

Table 2. Spectroscopic indices (field F588).

Star	Hβ	Mg	Mg1	Mg2	Mgb	MgH	Fe492	Fe498	Fe50	Fe53	Fe54
A-1	0.77	0.84	0.81	1.02	0.77	0.68	0.67	0.89	0.83	0.69	0.63
A-2	0.07	1.11	1.16	1.28	0.96	1.13	0.73	1.01	0.96	0.87	0.83
A-3	0.95	0.82	0.81	0.89	0.83	0.77	0.72	0.92	0.81	0.84	0.78
A-4	0.84	1.09	1.05	1.20	0.73	1.13	0.74	0.94	0.81	0.96	0.84
A-5	0.64	0.84	0.85	0.93	0.88	0.65	0.72	0.87	0.81	0.83	0.80
A-6	1.00	1.13	1.07	1.21	0.82	1.21	0.66	0.84	0.89	0.92	0.86
A-7	0.69	1.01	0.98	1.08	0.71	0.95	0.69	0.83	0.82	0.95	0.85
A-8	0.72	0.97	0.99	1.04	0.91	0.68	0.72	0.87	0.83	0.70	0.81
A-9	0.77	1.20	1.16	1.26	0.89	1.08	0.59	0.95	0.86	0.89	0.79
A-10	0.78	0.95	0.89	1.04	0.94	0.72	0.62	1.16	0.85	0.87	0.81
A-11	0.94	0.94	0.94	1.14	0.87	0.84	0.60	0.93	0.73	0.76	0.79
A-12	0.51	1.00	1.13	1.20	1.06	0.85	0.47	0.69	0.71	0.91	0.92
A-13	0.64	0.87	0.79	1.01	0.85	0.62	0.63	0.91	0.76	0.81	0.80
A-14	0.91	0.95	0.88	1.15	0.87	0.64	0.65	0.73	0.77	0.83	0.78
A-15	0.70	0.99	0.86	1.06	0.77	0.80	0.63	0.84	0.81	0.83	0.78
A-16	0.80	0.98	0.84	1.11	0.81	0.80	0.75	0.98	0.94	0.84	0.78
A-17	0.88	1.04	1.06	1.12	0.87	0.85	0.65	0.84	0.84	0.86	0.87
A-18	0.32	1.15	1.36	1.37	1.03	1.01	0.62	0.90	0.74	0.90	0.87
A-19	0.47	1.16	1.06	1.26	0.93	0.95	0.65	0.75	0.74	0.88	0.81
A-20	0.75	1.18	1.05	1.16	0.82	1.14	0.79	1.04	0.90	0.91	0.86
A-21	0.79	0.93	0.87	1.02	0.98	0.73	0.69	0.83	0.75	0.92	0.83
A-22	0.88	1.01	1.25	1.11	1.11	1.24	0.73	0.97	0.84	0.98	0.82
A-23	0.84	1.08	1.06	1.14	0.90	1.04	0.73	0.95	0.84	0.89	0.83
A-24	0.61	1.01	1.21	1.25	0.79	1.09	0.91	1.52	1.01	1.00	0.87
A-25	0.73	1.08	1.10	1.17	1.08	1.01	0.54	0.88	0.78	0.94	0.81
A-25	0.80	1.11	1.13	1.28	0.85	1.32	0.69	0.77	0.74	0.99	0.83
A-26	0.74	1.05	1.06	1.16	0.92	1.06	0.71	0.70	0.78	0.94	0.77
A-27	0.80	0.94	0.94	1.03	0.91	0.88	0.75	0.96	0.85	0.90	0.83
A-28	0.72	1.00	0.97	1.12	0.97	0.87	0.69	0.77	0.77	0.92	0.83
A-29	0.85	1.00	0.94	1.08	0.97	0.73	0.73	0.80	0.79	0.94	0.84
A-31	0.75	0.81	0.72	0.91	0.72	0.59	0.66	0.85	0.75	0.74	0.78
A-32	0.75	0.86	0.75	0.95	0.92	0.62	0.69	1.02	0.79	0.81	0.79
A-33	0.79	1.23	1.19	1.32	0.82	1.15	0.68	0.94	0.83	0.89	0.80
A-34	0.88	0.89	0.88	1.05	0.90	0.72	0.66	0.93	0.88	0.73	0.82
A-35	0.84	0.93	0.90	1.02	0.83	0.94	0.72	0.87	0.82	0.84	0.80
A-36	0.52	1.02	0.93	1.06	0.81	0.76	0.76	0.90	0.83	0.82	0.71
A-37	0.66	1.20	1.20	1.31	0.89	1.10	0.68	0.99	0.89	0.75	0.67
A-38	0.77	1.12	1.09	1.18	0.93	0.75	0.63	0.84	0.84	0.75	0.80
A-39	0.79	1.10	1.01	1.17	0.63	1.12	0.71	1.01	0.95	0.91	0.91
A-40	0.87	0.91	0.89	1.03	0.86	0.71	0.68	0.87	0.83	0.76	0.76
A-41	0.77	1.10	1.07	1.19	1.03	0.91	0.78	0.84	0.79	0.93	0.86
A-42	0.81	1.03	1.02	1.07	0.87	1.03	0.75	0.95	0.85	0.87	0.81
A-43	0.77	1.03	0.93	1.03	0.90	0.69	0.76	0.82	0.81	0.90	0.82
A-44	0.73	1.05	1.29	1.36	0.81	1.12	0.72	0.73	0.89	0.89	0.83
A-45	0.85	1.03	1.06	1.12	1.06	0.68	0.77	0.87	0.83	0.86	0.82
A-46	0.86	1.27	1.27	1.25	0.92	1.17	0.74	0.85	0.74	1.03	0.84
A-47	0.67	1.10	1.01	1.21	0.79	0.87	0.66	0.85	0.76	0.84	0.80
A-48	0.74	0.96	0.95	1.14	0.83	0.79	0.68	0.83	0.80	0.90	0.76

Table 2 – *continued*

Star	Hβ	Mg	Mg1	Mg2	Mgb	MgH	Fe492	Fe498	Fe50	Fe53	Fe54
A-49	0.76	1.08	1.06	1.17	0.83	1.05	0.64	0.84	0.83	0.93	0.82
A-50	0.84	1.13	1.12	1.25	0.90	0.92	0.71	0.87	0.83	0.81	0.79
A-51	0.84	1.10	1.08	1.27	1.09	0.73	0.77	0.90	0.81	0.90	0.86
A-52	0.70	0.99	0.95	1.10	0.92	0.73	0.59	0.88	0.82	0.87	0.81
A-53	0.94	1.15	1.09	1.24	0.78	0.93	0.71	0.93	0.91	0.80	0.88
A-55	0.75	1.07	1.00	1.04	0.89	0.79	0.76	0.82	0.79	0.93	0.84
A-56	0.79	0.94	0.84	1.02	0.82	0.70	0.68	0.90	0.82	0.80	0.78
A-57	0.71	1.09	1.06	1.22	0.94	1.06	0.67	0.83	0.74	0.95	0.81
A-58	0.90	0.90	0.88	0.99	0.83	0.70	0.69	0.96	0.83	0.75	0.81
A-59	0.69	0.89	0.90	1.00	0.72	0.71	0.68	0.78	0.80	0.80	0.84
A-60	0.64	1.02	1.03	1.13	0.88	0.79	0.73	0.81	0.80	0.74	0.81
A-61	0.87	1.06	1.06	1.18	0.85	1.12	0.70	0.91	0.84	0.92	0.79
A-62	0.66	1.20	1.21	1.31	0.92	0.92	0.58	0.80	0.81	0.79	0.84
A-63	0.63	1.10	1.08	1.18	0.70	0.99	0.65	0.89	0.81	0.83	0.83
A-64	0.89	1.14	1.21	1.27	1.02	1.20	0.76	0.96	0.86	0.96	0.80
A-65	0.89	1.20	1.24	1.30	0.95	1.10	0.67	0.97	0.87	0.85	0.79
A-66	0.75	1.19	1.15	1.31	1.00	1.14	0.81	1.09	0.75	0.85	0.83
A-67	0.67	0.96	0.91	1.11	0.90	0.71	0.66	0.72	0.75	0.89	0.82
A-68	0.73	1.00	0.93	1.07	0.97	0.82	0.69	0.73	0.76	0.89	0.79
A-69	0.74	1.09	1.06	1.18	0.90	1.03	0.70	0.83	0.75	0.87	0.83
A-70	0.77	1.05	1.04	1.13	0.80	1.14	0.71	0.96	0.80	0.91	0.82
A-71	0.83	1.01	0.95	1.13	0.78	0.72	0.62	0.83	0.76	0.86	0.78
A-72	0.77	1.18	1.16	1.24	0.87	0.96	0.68	0.78	0.76	0.96	0.71
A-25	0.97	1.08	1.31	1.13	1.35	1.26	0.15	1.28	1.10	0.86	0.63
A-26	0.96	0.79	0.75	0.95	0.72	0.79	0.65	0.86	0.77	0.86	0.81
A-73	0.99	0.66	0.54	0.61	0.77	0.39	0.89	0.84	0.76	0.65	0.68
A-74	0.85	1.13	1.11	1.25	0.90	0.95	0.66	0.87	0.82	0.83	0.82
A-75	0.91	0.91	0.91	1.08	0.90	0.71	0.65	0.96	0.84	0.78	0.84
A-76	0.32	1.16	1.15	1.41	0.88	0.93	0.67	0.97	0.87	0.96	0.81
A-77	0.68	1.11	1.09	1.29	0.91	0.84	0.74	1.00	0.84	0.72	0.82
A-78	0.94	0.74	0.62	0.65	0.76	0.48	0.77	0.81	0.78	0.93	0.84
A-79	0.64	1.07	1.04	1.03	0.89	0.84	0.72	0.87	0.82	0.88	0.82
A-80	0.84	1.17	1.11	1.27	0.92	0.80	0.71	1.04	0.87	0.78	0.84
A-81	0.71	0.99	0.84	1.04	0.70	0.76	0.75	0.88	0.71	0.69	0.81
A-82	0.78	0.96	0.96	1.05	0.85	0.72	0.69	0.92	0.83	0.68	0.61
A-83	0.76	0.72	0.66	0.72	0.76	0.59	0.72	0.75	0.73	0.85	0.75
A-84	0.69	1.05	1.06	1.20	1.21	0.77	0.59	0.81	0.69	0.87	0.91
A-85	0.61	1.07	1.65	1.72	1.62	1.49	0.24	0.25	0.58	0.92	0.94
A-86	—	1.74	1.94	2.12	1.75	2.12	—	0.06	—	0.95	0.79
A-87	1.20	1.05	0.94	1.27	0.46	0.76	0.43	1.10	0.98	0.92	0.96
A-88	0.66	1.12	0.99	1.17	0.68	1.01	0.71	1.16	0.96	0.90	0.80
A-89	1.00	1.00	0.95	1.10	0.85	1.01	0.66	0.92	0.89	0.77	0.79
A-90	0.88	1.23	1.19	1.26	1.00	0.95	0.59	1.11	0.93	0.81	0.84
A-91	0.76	1.01	1.00	1.07	0.82	0.86	0.58	0.76	0.72	0.80	0.79
A-92	0.77	1.04	0.91	1.10	0.87	0.85	0.64	1.09	0.87	0.94	0.78
A-93	0.92	1.14	1.11	1.28	0.97	1.19	0.63	0.89	0.85	0.95	0.81
A-94	0.95	1.06	1.04	1.11	0.90	0.99	0.71	0.82	0.77	0.90	0.80
A-95	0.76	1.11	1.10	1.16	0.91	1.09	0.61	0.81	0.76	0.82	0.87
A-96	0.82	1.15	1.14	1.27	0.91	0.96	0.67	0.81	0.74	0.97	0.85

Table 2 – *continued*

Star	Hβ	Mg	Mg1	Mg2	Mgb	MgH	Fe492	Fe498	Fe50	Fe53	Fe54
A-25	0.82	0.79	0.68	0.92	0.94	0.62	0.70	1.04	0.78	0.84	0.79
A-97	0.76	0.74	0.67	0.75	0.85	0.47	0.78	0.91	0.82	0.85	0.76
A-98	1.35	1.00	0.95	1.16	0.94	1.09	0.81	0.86	0.81	0.71	0.76
A-99	2.93	0.85	0.91	0.92	1.08	0.62	0.08	—	0.82	1.09	0.88
A-100	0.48	0.95	0.96	1.16	1.07	0.73	0.56	0.89	0.94	0.90	0.87
A-101	1.59	0.35	0.10	0.57	0.19	0.71	1.24	—	0.80	1.83	1.41
A-102	0.96	0.56	0.46	0.44	0.71	0.27	0.77	0.74	0.77	1.09	0.83
A-103	0.78	1.12	1.15	1.06	0.85	1.04	0.67	0.70	0.86	0.94	0.96
A-104	0.93	1.14	1.40	1.23	1.21	1.16	0.41	0.97	1.01	0.68	0.66
A-105	0.63	0.89	0.74	0.98	0.69	0.82	0.74	1.32	0.88	0.67	0.86
A-106	0.79	0.97	1.01	1.10	1.01	1.11	0.42	0.97	0.86	0.83	0.77
A-107	0.81	0.82	0.71	0.84	0.78	0.63	0.73	0.83	0.77	0.88	0.85
A-108	0.40	1.39	1.31	1.48	0.66	0.77	0.55	0.93	0.76	0.77	0.79
A-109	0.45	1.56	1.35	1.45	1.76	0.40	0.97	0.25	0.91	1.02	0.61
A-110	1.21	1.03	—	—	—	4.57	1.44	0.56	0.69	0.90	0.67
A-111	3.49	1.12	1.25	2.51	0.10	2.08	—	—	1.13	0.83	0.75
A-112	0.98	1.17	1.13	1.34	1.19	0.77	0.52	1.38	0.96	0.93	0.77
A-113	1.30	1.22	1.24	1.44	1.01	1.08	0.79	0.99	0.84	0.87	0.87
A-114	0.83	0.98	1.17	1.22	0.77	1.25	1.45	1.16	0.89	0.87	0.87
A-115	0.70	1.03	1.05	1.12	0.78	0.72	0.81	0.93	0.90	0.90	0.70
A-116	0.94	1.15	1.12	1.11	1.04	0.89	0.78	0.99	0.92	0.87	0.78
A-117	0.87	0.94	0.90	1.05	0.85	0.68	0.78	0.88	0.82	0.77	0.76
A-118	0.84	1.10	1.08	1.11	1.06	0.74	0.99	1.06	0.92	0.78	0.73
A-119	0.61	2.02	1.96	1.80	2.22	1.12	—	—	0.02	1.19	0.88
A-120	1.42	1.10	1.02	1.16	1.02	0.70	0.58	0.68	0.79	0.90	0.86
B-1	0.88	0.98	0.97	1.14	0.83	0.73	0.69	0.94	0.86	0.78	0.81
B-2	0.66	0.95	0.93	1.13	0.75	0.68	0.73	1.00	0.84	0.89	0.81
B-3	0.59	0.97	0.96	1.26	0.56	1.08	0.52	0.99	1.10	0.76	1.01
B-4	0.69	1.22	1.15	1.36	0.81	0.97	0.62	0.91	0.87	0.97	0.88
B-5	0.69	1.07	0.99	1.23	0.93	0.87	0.69	0.91	0.84	0.89	0.88
B-6	0.61	1.02	1.26	1.46	0.91	1.29	0.57	0.84	0.87	0.96	0.85
B-7	0.60	1.16	1.11	1.25	0.97	0.91	0.65	1.03	0.83	0.76	0.78
B-8	0.72	0.99	0.95	1.14	0.96	0.73	0.63	0.85	0.78	0.82	0.82
B-9	0.85	1.04	1.03	1.18	0.89	0.80	0.69	0.94	0.87	0.78	0.81
B-10	0.86	1.12	1.12	1.26	0.83	0.91	0.65	0.88	0.80	0.81	0.81
B-11	0.52	1.18	1.95	2.23	0.78	2.07	0.45	1.23	1.17	0.95	0.80
B-12	0.59	1.05	1.04	1.22	0.76	0.85	0.73	0.69	0.84	0.93	0.81
B-13	0.70	1.04	0.94	1.12	0.93	0.74	0.67	0.84	0.78	0.95	0.83
B-14	0.84	1.05	1.04	1.16	0.89	1.10	0.68	0.90	0.83	0.90	0.83
B-15	0.73	1.06	1.05	1.17	0.83	0.84	0.68	0.95	0.87	0.92	0.84
B-16	0.79	1.12	1.22	1.24	0.94	1.12	0.48	1.17	1.04	0.83	0.76
B-17	0.79	1.07	0.99	1.18	0.84	0.84	0.72	0.90	0.81	0.92	0.85
B-18	0.62	0.75	0.85	0.94	0.68	1.01	0.48	1.08	0.72	0.82	0.83
B-19	0.76	0.97	0.91	1.14	0.93	0.72	0.63	0.93	0.83	0.88	0.80
B-20	0.70	1.19	1.12	1.29	0.98	1.00	0.73	0.96	0.92	0.89	0.83
B-21	0.71	0.99	0.90	1.11	0.97	0.70	0.68	0.91	0.83	0.82	0.80
B-22	0.89	1.08	1.11	1.23	0.95	0.97	0.76	1.00	0.84	0.92	0.80
B-23	0.72	1.12	1.06	1.29	0.95	0.89	0.62	0.90	0.76	0.85	0.81
B-24	0.83	0.98	0.89	1.19	0.88	0.75	0.66	0.89	0.82	0.86	0.81
B-25	0.51	1.12	1.28	1.43	0.89	1.07	0.79	0.88	0.91	0.86	0.83

Table 2 – *continued*

Star	Hβ	Mg	Mg1	Mg2	Mgb	MgH	Fe492	Fe498	Fe50	Fe53	Fe54
B-26	0.71	1.17	1.25	1.31	1.14	1.21	0.34	1.14	0.97	0.87	0.70
B-27	0.92	0.94	0.91	1.08	0.83	0.86	0.71	0.91	0.86	0.85	0.79
B-28	0.73	0.91	0.88	1.13	0.83	0.87	0.65	0.96	0.84	0.83	0.78
B-29	0.93	1.20	1.11	1.33	0.90	0.94	0.73	1.05	0.81	0.93	0.85
B-30	0.84	1.35	1.53	1.62	1.04	1.38	0.68	0.77	1.04	0.93	0.87
B-31	0.75	1.16	1.11	1.25	0.80	0.91	0.66	0.87	0.83	0.80	0.78
B-32	0.84	1.10	1.10	1.23	0.95	1.05	0.71	0.93	0.83	0.87	0.85
B-33	0.66	1.08	1.01	1.22	0.86	0.84	0.73	0.94	0.83	0.84	0.83
B-34	0.85	1.24	1.34	1.35	1.01	1.15	0.51	1.01	0.96	0.79	0.76
B-35	0.75	1.30	1.30	1.44	0.92	1.15	0.68	0.99	0.91	0.89	0.78
B-36	0.89	1.24	1.26	1.39	0.94	1.20	0.59	0.98	0.87	0.97	0.81
B-37	0.83	0.92	0.82	1.03	0.76	0.60	0.72	0.84	0.80	0.85	0.79
B-38	0.85	1.05	1.04	1.15	0.88	1.07	0.68	0.96	0.86	0.80	0.83
B-39	0.78	1.18	1.16	1.27	0.96	1.09	0.46	1.06	0.89	0.94	0.76
B-40	1.00	1.05	1.06	1.16	0.89	1.18	0.67	0.94	0.83	0.82	0.77
B-41	0.78	0.94	0.88	1.08	0.92	0.66	0.64	0.87	0.78	0.87	0.80
B-42	1.10	1.01	1.01	1.16	0.85	0.77	0.60	1.06	0.85	0.78	0.82
B-43	0.69	1.15	1.04	1.26	0.76	0.94	0.70	0.93	0.87	0.86	0.80
B-44	0.72	1.15	1.15	1.30	0.89	0.90	0.80	0.99	0.92	0.84	0.67
B-45	0.72	0.97	0.88	1.06	0.92	0.68	0.67	0.84	0.81	0.88	0.78
B-46	0.86	1.10	1.10	1.23	0.91	0.87	0.78	0.99	0.90	0.82	0.82
B-47	0.72	1.07	1.02	1.23	1.00	0.77	0.62	0.74	0.73	0.81	0.83
B-48	0.81	1.04	0.95	1.15	0.83	0.75	0.70	0.92	0.82	0.88	0.81
B-49	1.08	1.08	1.52	1.88	1.00	1.19	0.79	0.71	0.83	0.96	0.81
B-50	0.72	1.05	1.21	1.53	0.86	1.11	0.75	0.66	0.83	0.95	0.63
B-51	0.93	0.89	0.86	1.01	0.87	0.64	0.72	0.97	0.83	0.76	0.81
B-52	0.82	0.92	0.88	1.14	0.88	0.73	0.81	0.94	0.84	0.81	0.74
B-53	1.01	1.14	1.28	1.38	1.12	1.26	0.37	1.20	0.94	0.87	0.77
B-54	0.57	1.15	1.48	1.74	0.91	1.80	0.74	0.76	0.94	0.89	0.80
B-55	0.88	0.95	0.98	1.03	0.92	0.71	0.73	0.95	0.85	0.77	0.81
B-56	0.94	1.11	1.13	1.23	0.87	0.96	0.72	0.88	0.87	0.69	0.87
B-57	0.85	1.07	1.03	1.22	0.86	0.85	0.91	0.91	0.90	0.73	0.88
B-58	0.75	1.07	1.08	1.25	0.86	0.84	0.72	0.94	0.88	0.88	0.81
B-60	0.75	1.17	1.17	1.36	0.90	0.90	0.66	0.98	0.85	0.68	0.66
B-61	0.73	1.14	1.10	1.29	1.04	0.77	0.60	0.80	0.78	0.91	0.81
B-62	0.81	1.19	1.12	1.28	0.87	0.83	0.66	0.88	0.82	0.93	0.81
B-63	0.51	1.69	1.78	1.87	0.85	1.95	—	4.81	2.24	0.99	0.70
B-64	0.71	1.05	1.39	1.54	0.99	1.42	0.67	0.92	0.91	0.94	0.74
B-65	0.80	1.20	1.22	1.37	1.05	0.95	0.78	0.94	0.93	0.81	0.72
B-66	0.77	0.84	1.53	3.33	0.83	1.05	0.54	0.01	0.13	0.85	0.79
B-67	0.77	1.04	0.95	1.16	0.98	0.72	0.72	0.88	0.86	0.88	0.80
B-68	0.69	1.08	1.28	1.54	1.08	1.13	0.95	1.11	1.00	0.90	0.86
B-69	0.76	0.91	0.89	1.08	0.91	0.64	0.78	0.90	0.87	0.82	0.75
B-70	0.79	0.88	0.85	1.03	0.84	0.63	0.72	0.92	0.87	0.73	0.75
B-71	0.85	0.85	0.81	1.05	0.79	0.63	0.64	0.92	0.84	0.67	0.61
B-72	0.82	1.24	1.16	1.36	1.04	0.97	0.61	0.98	0.76	0.88	0.73
B-73	1.15	1.66	1.74	1.80	1.22	1.70	0.28	1.04	0.88	1.00	0.81
B-74	0.90	1.17	1.09	1.35	1.04	0.93	0.87	0.79	0.82	0.99	0.88
B-75	0.76	1.13	1.24	1.31	1.10	1.08	0.47	1.05	0.92	0.93	0.76
B-76	0.77	1.15	1.14	1.28	0.88	0.99	0.65	0.94	0.86	0.85	0.81

Table 2 – *continued*

Star	Hβ	Mg	Mg1	Mg2	Mgb	MgH	Fe492	Fe498	Fe50	Fe53	Fe54
B-77	0.73	1.13	1.19	1.34	0.93	1.04	0.55	0.79	0.76	0.90	0.82
B-78	0.61	1.02	1.77	1.82	1.16	1.54	0.09	0.78	0.81	0.98	0.87
B-79	0.98	1.00	1.04	1.04	1.01	0.74	0.66	0.85	0.81	0.61	0.67
B-80	0.75	1.09	1.06	1.26	1.04	0.81	0.59	0.85	0.72	0.85	0.85
B-81	0.68	1.10	1.02	1.32	0.79	1.32	0.73	1.16	0.77	0.84	0.80
B-82	0.71	1.19	1.11	1.35	0.82	0.97	0.63	0.93	0.83	0.85	0.84
B-83	—	—	—	—	—	—	—	—	—	—	—
B-84	0.92	1.12	1.15	1.25	0.84	0.90	0.61	0.92	0.88	0.78	0.83
B-85	0.74	1.00	0.95	1.13	0.99	0.76	0.65	0.82	0.76	0.89	0.82
B-86	0.87	0.96	0.95	1.09	0.85	0.74	0.64	0.91	0.84	0.78	0.81
B-87	0.90	1.05	1.05	1.15	0.82	1.07	0.55	0.94	0.84	0.91	0.78
B-88	0.78	0.81	0.72	1.01	0.87	0.60	0.70	0.89	0.82	0.80	0.75
B-89	0.73	0.95	0.91	1.11	0.96	0.75	0.72	0.89	0.83	0.84	0.82
B-90	0.83	1.00	0.98	1.12	0.86	0.77	0.65	0.91	0.87	0.84	0.86
B-91	0.68	1.15	1.06	1.23	0.82	0.84	0.64	0.97	0.84	0.91	0.81
B-92	0.21	1.03	1.36	1.43	0.87	1.35	0.83	1.29	1.07	0.85	0.80
B-93	0.83	1.07	1.07	1.19	0.90	0.94	0.67	0.89	0.84	0.84	0.80
B-94	0.82	1.18	1.17	1.33	0.80	1.09	0.63	1.10	0.92	0.82	0.77
B-95	0.94	1.16	1.12	1.33	0.84	1.20	0.66	0.87	0.80	0.84	0.83
B-96	0.95	1.25	1.31	1.34	1.16	1.28	0.31	1.23	1.04	0.98	0.76
B-97	0.68	1.40	1.38	1.63	1.07	1.18	0.34	0.99	0.84	0.93	0.77
B-98	0.73	1.15	1.10	1.28	0.77	1.06	0.58	1.04	0.90	1.03	0.92
B-99	0.85	0.87	0.85	1.04	0.80	0.60	0.68	0.94	0.87	0.72	0.76
B-100	0.70	0.98	0.96	1.10	0.82	0.77	0.79	0.94	0.90	0.86	0.77
B-101	0.72	0.96	0.91	1.08	0.94	0.68	0.68	0.86	0.76	0.84	0.81
B-102	0.35	1.10	1.47	1.49	0.82	1.68	1.11	1.09	1.06	0.91	0.63
B-103	0.87	0.92	0.95	1.01	0.96	0.72	0.67	0.92	0.84	0.78	0.82
B-104	0.69	1.17	1.27	1.32	1.17	0.79	0.68	0.92	0.89	0.80	0.69
B-105	0.80	1.15	1.18	1.26	0.92	1.19	0.63	0.95	0.82	0.96	0.84
B-106	0.80	1.23	1.33	1.39	1.17	1.27	0.40	1.07	0.95	0.93	0.73
B-107	0.92	—	—	—	0.15	—	0.79	0.54	0.66	0.89	0.88
B-108	0.73	0.99	0.92	1.06	0.80	0.69	0.63	0.88	0.82	0.82	0.80
B-109	0.70	1.23	1.26	1.38	0.92	1.13	0.53	0.95	0.88	0.92	0.72
B-110	0.84	1.09	1.06	1.21	0.86	1.01	0.64	0.89	0.82	0.81	0.82
B-111	0.86	1.07	1.08	1.18	0.82	1.10	0.54	0.98	0.84	0.81	0.78
B-112	0.72	0.93	0.86	1.05	0.93	0.72	0.60	0.85	0.76	0.84	0.79
B-113	0.76	1.10	1.03	1.24	1.00	0.90	0.66	1.11	0.82	0.90	0.80
B-114	0.88	1.17	1.35	1.24	1.13	1.18	0.44	1.09	0.97	0.79	0.65
B-115	0.74	1.09	1.08	1.24	0.86	0.84	0.71	0.89	0.84	0.86	0.84
B-116	0.01	1.20	1.89	2.01	0.96	1.46	0.70	0.80	0.99	0.94	0.89
B-117	0.84	1.15	1.08	1.27	0.85	0.94	0.67	0.89	0.79	0.98	0.80
B-118	0.72	1.04	1.03	1.20	0.89	0.66	0.63	0.90	0.87	0.67	0.77
B-119	0.63	1.07	1.12	1.33	0.93	1.02	0.50	0.89	0.81	0.85	0.84
B-120	0.78	1.10	1.06	1.19	0.87	0.94	0.61	0.89	0.82	0.93	0.81
13-06	0.82	1.14	0.71	—	—	—	0.65	—	0.79	0.83	—
13-18	0.89	1.18	0.94	—	—	—	0.69	—	0.83	0.84	—
13-20	0.88	1.07	0.80	—	—	—	0.69	—	0.76	0.94	—
13-25	0.89	0.92	0.84	—	—	—	0.76	—	0.80	0.83	—
13-26	0.94	0.84	0.79	—	—	—	0.75	—	0.80	0.76	—
13-33	0.88	0.99	0.78	—	—	—	0.71	—	0.81	0.82	—

Table 2 – *continued*

Star	Hβ	Mg	Mg1	Mg2	Mgb	MgH	Fe492	Fe498	Fe50	Fe53	Fe54
13-35	0.90	1.04	0.81	—	—	—	0.77	—	0.86	0.79	—
13-37	0.84	0.96	0.83	—	—	—	0.73	—	0.81	0.81	—
13-41	0.77	1.13	0.76	—	—	—	0.55	—	0.86	0.89	—
13-43	0.78	1.18	0.87	—	—	—	0.67	—	0.83	0.91	—
13-47	0.90	1.05	0.90	—	—	—	0.71	—	0.83	0.95	—
13-48	0.86	0.98	0.98	—	—	—	0.68	—	0.82	0.85	—
13-50	0.90	1.12	0.91	—	—	—	0.78	—	0.81	0.83	—
13-52	0.93	0.92	0.86	—	—	—	0.82	—	0.81	0.82	—
13-59	0.85	1.06	0.90	—	—	—	0.68	—	0.87	0.80	—
61-08	0.87	1.06	0.86	—	—	—	0.72	—	0.83	0.94	—
61-14	0.91	0.84	—	—	—	—	0.61	—	0.76	0.82	—
61-20	0.82	0.95	0.84	—	—	—	0.63	—	0.83	0.86	—
61-21	0.90	1.00	0.84	—	—	—	0.69	—	0.84	0.92	—
61-27	0.76	0.84	0.93	—	—	—	—	—	0.72	0.77	—
61-28	0.84	1.09	0.93	—	—	—	0.65	—	0.87	0.91	—
61-32	—	0.90	0.90	—	—	—	0.65	—	0.86	0.81	—
61-35	0.86	0.92	0.79	—	—	—	0.73	—	0.85	0.89	—
61-37	0.85	1.01	0.80	—	—	—	0.65	—	0.86	0.92	—
61-39	0.80	0.98	0.74	—	—	—	0.70	—	0.81	0.90	—
61-40	0.75	0.78	0.60	—	—	—	0.63	—	0.78	0.90	—
61-43	0.81	0.94	0.69	—	—	—	0.75	—	0.87	0.80	—
61-45	0.88	0.98	0.87	—	—	—	0.72	—	0.84	0.94	—
61-47	0.86	1.10	0.75	—	—	—	0.68	—	0.79	0.96	—
61-52	0.84	0.99	0.88	—	—	—	0.60	—	0.76	0.94	—
61-53	—	1.14	0.68	—	—	—	—	—	0.78	0.80	—
61-55	0.85	0.94	0.66	—	—	—	0.72	—	0.81	0.88	—
61-61	0.85	0.97	0.82	—	—	—	0.69	—	0.83	0.93	—
61-64	0.92	1.00	0.78	—	—	—	0.80	—	0.78	0.95	—
61-68	0.82	1.09	0.84	—	—	—	0.63	—	0.83	0.86	—
9-09	0.82	1.02	0.87	—	—	—	0.72	—	0.81	0.91	—
9-10	0.75	1.01	0.79	—	—	—	0.80	—	0.84	0.76	—
9-11	0.87	0.95	0.87	—	—	—	0.76	—	0.81	0.82	—
9-16	0.86	0.96	0.81	—	—	—	0.74	—	0.79	0.81	—
9-17	0.83	0.89	0.84	—	—	—	0.73	—	0.80	0.82	—
9-20	0.86	1.12	0.86	—	—	—	0.68	—	0.88	0.89	—
9-23	0.99	1.02	0.87	—	—	—	0.74	—	0.90	0.84	—
9-24	0.81	0.86	0.83	—	—	—	0.75	—	0.86	0.81	—
9-28	0.87	0.85	0.78	—	—	—	0.77	—	0.78	0.78	—
9-36	0.84	1.04	0.82	—	—	—	0.74	—	0.75	0.84	—
9-37	0.90	1.10	0.92	—	—	—	0.72	—	0.82	0.88	—
9-38	0.85	0.94	0.83	—	—	—	0.83	—	0.85	0.75	—
9-39	0.84	0.90	0.89	—	—	—	0.75	—	0.81	0.81	—
9-41	0.89	1.04	0.92	—	—	—	0.66	—	0.84	0.90	—
9-43	0.81	0.69	0.83	—	—	—	0.75	—	0.84	0.77	—
9-45	0.84	1.02	0.89	—	—	—	0.68	—	0.84	0.85	—
9-46	0.86	0.83	0.86	—	—	—	0.77	—	0.79	0.80	—
9-48	0.86	0.85	0.94	—	—	—	0.72	—	0.79	0.77	—
9-50	0.91	0.68	0.70	—	—	—	0.65	—	0.79	0.77	—
9-51	0.90	0.92	0.90	—	—	—	0.77	—	0.84	0.87	—
9-57	0.78	0.85	0.79	—	—	—	0.64	—	0.79	0.81	—

Table 2 – *continued*

Star	Hβ	Mg	Mg1	Mg2	Mgb	MgH	Fe492	Fe498	Fe50	Fe53	Fe54
9-60	0.78	0.81	0.77	—	—	—	0.72	—	0.80	0.83	—
9-64	0.79	1.09	0.83	—	—	—	0.61	—	0.87	0.87	—
20-01	0.80	0.97	—	—	—	—	0.74	—	—	—	—
20-02	0.94	1.06	—	—	—	—	0.53	—	0.88	—	—
23-01	0.89	1.06	—	—	—	—	0.48	—	0.91	—	—
23-02	0.90	0.99	—	—	—	—	0.71	—	—	—	—
25-01	—	0.89	—	—	—	—	0.75	—	—	—	—
25-02	0.78	0.89	—	—	—	—	0.70	—	0.80	—	—
27-01	0.90	1.06	—	—	—	—	0.72	—	0.81	—	—
27-02	0.91	1.04	—	—	—	—	0.59	—	0.85	—	—
29-01	0.89	0.88	—	—	—	—	0.68	—	0.78	—	—
29-02	0.88	1.01	—	—	—	—	0.62	—	0.81	—	—
41-01	0.98	0.85	—	—	—	—	0.68	—	0.81	—	—
41-02	0.97	0.92	—	—	—	—	0.69	—	0.80	—	—
43-01	0.95	1.06	—	—	—	—	0.60	—	0.86	—	—
43-02	0.97	0.88	—	—	—	—	0.71	—	0.83	—	—
43-03	0.93	0.77	—	—	—	—	0.68	—	0.79	—	—
45-01	0.90	0.89	—	—	—	—	0.70	—	0.80	—	—
45-02	0.93	0.90	—	—	—	—	0.79	—	0.80	—	—
45-03	0.98	1.10	—	—	—	—	0.69	—	0.83	—	—
47-01	0.95	0.99	—	—	—	—	0.68	—	0.81	—	—
47-02	0.95	0.83	—	—	—	—	0.70	—	0.80	—	—
129-01	0.92	1.00	—	—	—	—	0.59	—	0.84	—	—
129-02	0.86	1.03	—	—	—	—	0.56	—	0.81	—	—
131-01	0.91	1.04	—	—	—	—	0.63	—	0.83	—	—
131-03	0.89	0.81	—	—	—	—	0.67	—	0.79	—	—
133-01	0.87	0.97	—	—	—	—	0.70	—	0.79	—	—
137-01	0.88	0.93	—	—	—	—	0.72	—	0.79	—	—
139-01	0.90	0.94	—	—	—	—	0.69	—	0.82	—	—

Notes to table: Stellar IDs from this work. – means not measured.

There are 31 and 19 per cent of stars with higher than solar abundances in the fields F588 and M22, respectively. The observed percentage of metal-rich stars in the M22 field is a lower limit. These values contrast with that of 57 per cent found by Rich (1988), or with 34 per cent found by McWilliam & Rich (1994) in BW. There are almost no stars with higher than solar abundances in the field studied by Morrison & Harding (1993) at $(l, b)=(-10°, -10°)$ (the fraction is 0.15 per cent). Thus, the fraction of stars with higher than solar metallicity increases with decreasing Galactocentric distance, as expected.

There are 24 and 30 per cent of stars with [Fe/H]≤ -1 in the F588 and M22 fields, respectively. The observed percentage of metal-poor stars in M22 should be regarded as an upper limit, because, as argued above, there is a selection effect against including the most metal-rich stars. Morrison & Harding (1993) find 33 per cent of the stars in their field at $(l, b)=(-10°, -10°)$ have [Fe/H]≤ -1. According to the new abundance scale for BW (McWilliam & Rich 1994), ~12 per cent of the K giants have [Fe/H]≤ -1. Even though these estimates are based on different techniques for measuring [Fe/H], it is seen that the fraction of metal-poor stars increases with distance from the Galactic Centre, as expected.

The errors due to systematic differences between the various ways of measuring [Fe/H] are much more important than the Poisson errors in these fractions. However, it is reassuring that the fractions of metal-poor and metal-rich stars, as a function of distance, vary according to the expectations from the existence of a metallicity gradient in the Galactic bulge.

These numbers also show that the metal-rich stars have a steeper density law than the metal-poor stars. This result was also expected, as the M giants (which are predominantly metal-rich) show a steeper density law than the K giants (e.g. Frogel 1988). This result is also in agreement with the kinematic predictions, since the metal-poor stars have larger velocity dispersion than the metal-rich stars (Minniti 1995c). We will come back to the metallicity gradient in Section 6.

5 OTHER BULGE TRACERS

Given our results for the K giants, which are representative of all stars regardless of age and abundance (all stars go through the K giant phase), let us now make the comparison with other bulge tracers, which may represent just a narrow range of the parameter space. In making this comparison, we will also use kinematic information.

5.1 The RR Lyrae stars

The RR Lyrae stars in Baade's window have a mean metallicity [Fe/H] $= -1$ (Walker & Terndrup 1991). These abundances motivated Lee (1992) to conclude that the bulge is the oldest population in the Galaxy. However, Minniti (1995c)

Table 3. Spectroscopic indices (M22 field).

Star	Hβ	Mg	Mg1	Mg2	Mgb	MgH	Fe492	Fe498	Fe50	Fe52	Fe53	Fe54
86	0.84	0.86	0.72	0.78	0.77	0.55	0.65	0.86	0.79	0.75	0.67	1.19
408	1.26	0.85	0.83	1.16	0.84	0.75	1.06	0.79	0.77	0.75	0.66	0.89
467	0.85	0.79	0.76	1.00	0.79	0.76	0.65	0.95	0.80	0.78	0.80	0.75
681	0.93	0.80	0.69	0.82	0.82	0.60	0.71	0.87	0.76	0.78	0.77	0.94
385	0.86	0.84	0.75	0.67	0.81	0.78	0.75	0.81	0.80	0.81	0.72	0.98
386	0.84	0.84	0.72	0.67	0.79	0.68	0.72	0.81	0.75	0.76	0.71	0.86
203	0.75	0.85	0.73	0.76	0.77	0.72	0.67	0.83	0.77	0.76	0.77	1.06
510	0.76	0.76	0.64	0.57	0.87	0.64	0.70	0.87	0.81	0.81	0.75	1.02
292	0.79	0.80	0.76	0.90	0.88	0.61	0.64	0.83	0.73	0.84	0.82	0.79
383	0.83	0.85	0.71	0.72	0.87	0.60	0.69	0.88	0.82	0.83	0.83	0.95
494	0.75	0.98	0.95	1.20	0.85	0.69	0.69	0.96	0.86	0.86	0.62	0.66
500	0.79	0.93	0.87	1.07	0.85	0.72	0.62	0.88	0.77	0.79	0.81	0.80
637	0.87	0.91	0.88	1.06	0.80	0.74	0.67	0.88	0.84	0.87	0.76	0.79
41	0.77	0.87	0.77	1.02	0.88	0.65	0.62	0.91	0.80	0.83	0.83	0.77
53	0.90	0.92	0.88	1.09	0.82	0.69	0.68	0.95	0.83	0.82	0.75	0.78
392	0.76	1.05	1.03	1.26	0.86	0.84	0.69	1.00	0.87	0.85	0.72	0.65
320	0.77	0.96	0.90	0.88	0.90	0.83	0.69	0.86	0.81	0.81	0.86	1.18
315	1.01	0.85	0.74	0.62	0.86	0.68	0.68	0.99	0.83	0.86	0.84	0.95
403	0.73	0.86	0.80	1.04	0.92	0.64	0.66	0.90	0.79	0.84	0.83	0.77
411	0.90	0.90	0.89	0.90	0.89	0.81	0.65	0.79	0.79	0.85	0.82	0.91
610	0.81	0.92	0.84	0.80	0.81	0.80	0.59	0.83	0.81	0.80	0.82	0.46
578	0.78	0.96	0.87	0.81	0.90	0.84	0.65	0.92	0.80	0.81	0.79	0.99
218	0.91	0.96	1.12	0.81	1.13	1.30	0.23	1.26	1.11	0.87	0.78	0.44
571	0.77	0.94	0.80	0.76	0.92	0.70	0.71	0.85	0.84	0.83	0.78	1.21
690	0.79	0.88	0.78	0.76	0.89	0.74	0.69	0.82	0.82	0.84	0.84	1.01
703	0.85	0.98	0.90	0.92	0.87	0.88	0.57	0.85	0.82	0.80	0.83	0.48
196	0.79	1.07	0.98	0.94	0.94	0.91	0.67	0.86	0.80	0.83	0.79	0.96
511	0.79	0.99	0.87	0.83	0.93	0.77	0.68	0.80	0.81	0.84	0.83	1.13
114	0.80	0.89	0.87	1.06	0.80	0.64	0.69	0.93	0.84	0.85	0.77	0.82
314	0.76	1.02	0.92	0.87	0.89	0.83	0.75	0.84	0.80	0.80	0.77	0.94
39	0.76	0.97	0.85	1.08	0.75	0.76	0.65	0.91	0.82	0.78	0.86	0.81
567	0.83	0.92	0.80	0.75	0.88	0.67	0.71	0.85	0.82	0.82	0.84	1.08
714	0.82	0.98	0.88	0.80	0.88	0.83	0.75	0.81	0.86	0.88	0.80	1.08
18	0.75	1.11	1.11	1.24	0.92	0.90	0.66	1.03	0.87	0.88	0.69	0.69
717	0.78	1.11	1.08	1.02	0.93	1.09	0.52	0.90	0.84	0.81	0.85	1.06
6	0.71	0.97	0.88	1.06	0.81	0.70	0.67	0.90	0.81	0.81	0.86	0.79
591	0.69	0.80	0.70	0.92	0.85	0.59	0.64	0.84	0.76	0.89	0.82	0.78
307	0.81	0.96	0.85	0.84	0.89	0.71	0.71	0.78	0.82	0.85	0.84	1.08
36	0.82	0.98	0.88	1.04	0.76	0.72	0.73	0.87	0.82	0.81	0.83	0.85
303	0.77	1.08	0.99	0.91	0.92	0.92	0.71	0.84	0.80	0.84	0.81	1.02
84	0.80	1.05	0.94	0.89	0.93	0.78	0.69	0.87	0.82	0.83	0.77	1.10
721	0.79	0.94	0.80	0.79	0.91	0.69	0.72	0.87	0.82	0.85	0.85	1.02
662	0.83	1.04	0.90	0.92	0.84	0.71	0.59	0.89	0.83	0.80	0.76	0.34
726	0.76	0.96	0.82	0.82	0.84	0.72	0.74	0.86	0.82	0.86	0.79	0.88
50	0.74	1.04	0.94	1.18	0.80	0.82	0.65	0.88	0.80	0.81	0.86	0.80
719	0.85	0.95	0.95	0.91	0.92	0.95	0.64	0.85	0.82	0.86	0.91	1.04
393	0.82	0.93	0.82	0.72	0.89	0.76	0.74	0.79	0.81	0.86	0.85	1.12
140	0.75	1.02	0.91	1.16	0.83	0.70	0.71	0.97	0.86	0.80	0.86	0.79
516	0.80	1.04	1.01	0.93	0.95	1.02	0.59	0.81	0.82	0.78	0.84	1.08
607	0.75	0.95	0.85	1.05	0.93	0.76	0.66	1.04	0.79	0.84	0.89	0.81
148	0.78	1.05	0.99	0.93	0.90	0.97	0.62	0.81	0.79	0.88	0.91	1.00
101	0.70	1.01	0.99	1.20	0.91	0.74	0.64	0.84	0.83	0.88	0.87	0.79
577	0.84	1.22	1.42	0.99	1.27	1.25	0.26	1.08	1.01	0.75	0.74	1.00
689	0.75	1.09	0.98	0.96	0.96	0.95	0.64	0.88	0.84	0.85	0.85	1.14
691	0.79	1.06	0.98	0.90	0.90	0.96	0.73	0.83	0.81	0.87	0.88	1.01
13	0.92	1.06	1.04	1.25	0.94	0.79	0.75	0.99	0.93	0.90	0.82	0.82

Table 3 – *continued*

Star	Hβ	Mg	Mg1	Mg2	Mgb	MgH	Fe492	Fe498	Fe50	Fe52	Fe53	Fe54
371	0.83	1.00	0.88	0.84	0.89	0.76	0.72	0.85	0.81	0.85	0.80	1.06
7	0.84	1.11	1.02	1.19	0.84	0.81	0.67	0.93	0.82	0.83	0.85	0.82
156	0.77	1.04	0.98	0.92	0.90	0.97	0.67	0.81	0.80	0.92	0.87	0.94
279	0.74	1.06	1.07	1.23	0.83	0.86	0.66	0.89	0.81	0.90	0.87	0.81
52	0.75	1.09	0.99	1.19	0.81	0.82	0.70	0.92	0.84	0.83	0.89	0.83
152	0.77	1.14	1.08	0.96	0.95	0.90	0.56	0.86	0.85	0.90	0.90	0.88
308	0.78	1.06	0.95	0.91	0.91	0.81	0.67	0.79	0.80	0.88	0.90	0.99
29	0.78	0.98	0.98	1.12	0.83	0.77	0.61	0.88	0.83	0.86	0.81	0.69
211	0.90	1.10	1.10	1.22	0.90	1.04	0.67	0.92	0.83	0.90	0.86	0.84
522	0.70	1.09	0.99	1.15	0.98	0.79	0.64	0.82	0.78	0.93	0.89	0.85
328	0.65	1.25	1.20	1.49	1.08	0.98	0.55	1.08	0.95	0.90	0.89	0.82
618	0.80	0.95	0.87	0.78	0.90	0.85	0.60	0.84	0.82	0.89	0.92	0.54
231	0.68	1.29	1.24	1.47	1.13	1.08	0.56	0.99	0.89	0.84	0.88	0.80
687	0.86	0.87	0.81	0.73	0.86	0.75	0.71	0.80	0.78	0.84	0.86	0.98
402	0.77	1.14	1.08	1.00	0.93	1.07	0.65	0.87	0.82	0.91	0.83	0.99
318	0.74	0.97	0.94	1.11	0.97	0.81	0.64	0.84	0.83	1.16	0.90	0.84
300	0.97	1.01	0.99	1.11	0.87	0.74	0.69	0.94	0.88	0.83	0.82	0.82
139	0.74	0.97	0.90	1.15	0.94	0.72	0.66	0.87	0.82	0.90	0.89	0.82
40	0.91	1.07	1.05	1.27	0.87	0.80	0.60	0.97	0.85	0.85	0.84	0.85
588	0.86	0.97	1.14	0.83	1.29	1.12	0.27	1.23	1.08	0.84	0.79	0.94
425	0.65	1.15	1.09	1.06	0.88	1.21	0.63	0.80	0.80	0.87	0.90	1.04
58	0.78	0.96	0.83	0.79	0.94	0.70	0.71	0.82	0.80	0.85	0.85	0.99
275	0.90	0.76	1.05	0.61	1.37	1.41	0.23	1.65	1.37	0.82	0.64	0.72
33	0.80	1.19	1.17	1.29	0.85	0.96	0.41	1.02	0.87	0.72	0.82	0.71
36	0.91	1.15	1.40	1.25	1.28	1.47	0.25	1.46	1.20	0.79	0.75	0.60
584	0.90	0.70	0.68	0.73	0.69	0.68	0.66	0.81	0.79	0.76	0.79	0.97
575	0.80	0.78	0.67	0.69	0.80	0.69	0.67	0.80	0.77	0.77	0.78	0.97
277	0.83	1.05	1.13	0.92	1.08	1.12	0.40	1.03	0.95	0.81	0.79	0.92
410	0.76	1.07	1.01	0.98	0.97	0.94	0.51	0.88	0.86	0.84	0.85	1.02
590	0.84	1.12	1.16	1.20	0.95	1.09	0.53	0.92	0.87	0.88	0.85	0.78
161	0.78	1.12	1.02	1.00	0.91	0.92	0.46	0.86	0.84	0.86	0.89	0.55
41	0.76	1.10	1.11	1.24	1.06	1.03	0.48	0.96	0.84	0.90	0.87	0.75
373	0.65	1.16	1.18	1.39	0.88	0.96	0.55	0.92	0.85	0.90	0.89	0.80
412	0.80	1.10	1.08	0.96	1.02	1.15	0.48	0.94	0.90	0.84	0.89	1.11
515	0.77	1.15	1.13	1.01	0.99	1.08	0.53	0.87	0.90	0.80	0.86	1.11
494	0.75	0.98	0.95	1.20	0.85	0.69	0.69	0.96	0.86	0.86	0.62	0.66
500	0.79	0.93	0.87	1.07	0.85	0.72	0.62	0.88	0.77	0.79	0.81	0.80
392	0.76	1.05	1.03	1.26	0.86	0.84	0.69	1.00	0.87	0.85	0.72	0.65
637	0.87	0.91	0.88	1.06	0.80	0.74	0.67	0.88	0.84	0.87	0.76	0.79
19	0.89	1.12	1.09	1.33	0.85	0.89	0.64	0.96	0.86	0.85	0.78	0.78
424	0.71	1.20	1.23	1.40	0.88	1.00	0.58	0.94	0.85	0.86	0.88	0.78
61	0.78	1.14	1.13	1.01	0.98	1.09	0.55	0.90	0.86	0.86	0.89	1.01
426	0.79	0.96	0.86	0.78	0.89	0.74	0.73	0.82	0.80	0.83	0.77	0.94
27	0.82	1.10	1.09	1.31	0.90	0.80	0.72	0.93	0.85	0.91	0.79	0.81
274	1.03	0.78	0.68	0.65	0.75	0.71	0.69	0.77	0.76	0.77	0.81	1.24
478	0.82	0.77	0.62	0.63	0.74	0.57	0.75	0.88	0.79	0.69	0.65	0.98
215	0.80	0.80	0.67	0.73	0.80	0.61	0.56	0.78	0.78	0.78	0.78	0.37
12	0.80	0.83	0.73	0.66	0.79	0.71	0.74	0.71	0.78	0.78	0.75	1.22
720	0.83	0.80	0.66	0.69	0.76	0.59	0.66	0.84	0.77	0.74	0.69	1.04
574	1.05	0.75	0.63	0.67	0.75	0.64	0.65	0.79	0.74	0.74	0.75	1.10
85	0.81	0.85	0.74	0.66	0.76	0.72	0.73	0.79	0.78	0.75	0.73	1.05
55	0.80	0.74	0.64	0.65	0.76	0.58	0.67	0.82	0.77	0.76	0.77	1.09
367	0.80	0.97	0.88	0.82	0.86	0.83	0.70	0.87	0.82	0.85	0.84	1.25
555	0.86	1.47	1.85	0.88	1.85	1.15	0.66	0.77	0.89	0.65	0.87	1.65
572	0.85	0.75	0.63	0.66	0.75	0.60	0.61	0.80	0.73	0.75	0.69	0.97
42	0.81	0.79	0.72	0.98	0.88	0.58	0.59	0.90	0.75	0.77	0.79	0.72

Notes to table: stellar IDs from Cudworth (1986).

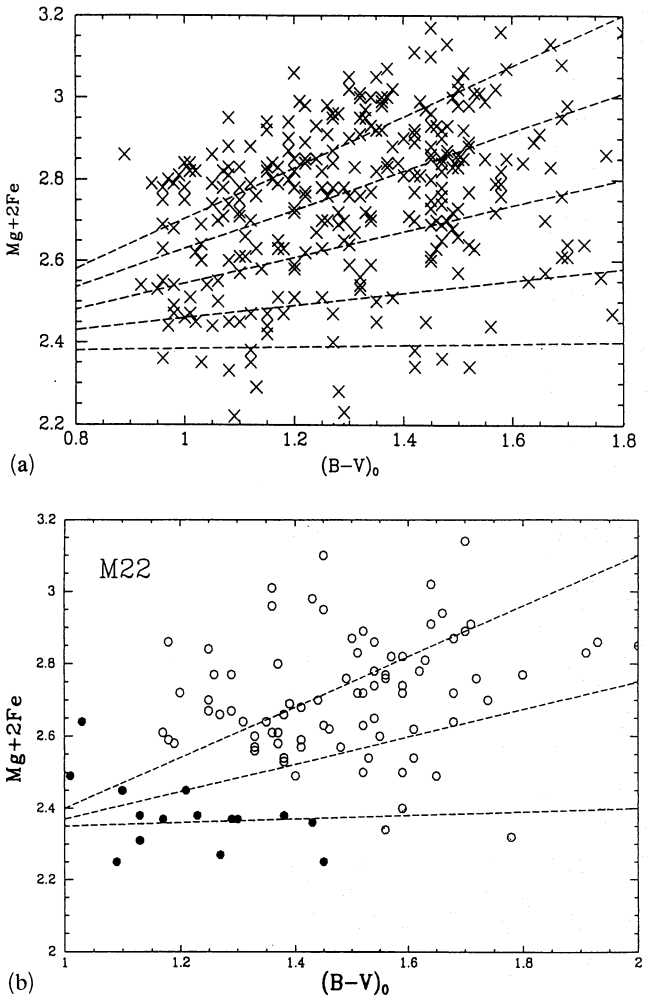

Figure 2. Combined index Mg + 2Fe versus dereddened $B-V$ colour for the K giants observed in the fields (a) F588 and (b) M22. The isoabundance lines in (a) correspond to [Fe/H] = −1.75, −1.5, −1.0, −0.5 and 0.0, from bottom to top. In (b) the dashed line indicates the locus of giants in three typical globular clusters.

argued that the RR Lyrae stars show halo-like kinematics, implying that the inner halo is old, but the bulk of the bulge population could be younger. A confirmation of the mean abundances and abundance ranges in different bulge fields (McWilliam & Rich 1994; this work) reveals that the RR Lyrae stars represent just the metal-poor tail of the bulge metallicity distribution, consistent with their being mostly halo members.

5.2 The M giants

The distribution of the M giants in the bulge is much more concentrated than that of the K giants (Terndrup 1988; Blanco & Terndrup 1989). In general, the M giants have kinematics representative of the metal-rich bulge population (Minniti 1995c). Even within M giants of different types, there is a marked spatial segregation: the M giants of later spectral types show much more concentrated distribution towards the Galactic Centre than the early M giants. Increasing spectral types of these cool giants are thought to be positively correlated with increasing metal content. Thus, later M giants have a predominantly metal-rich origin. The fact that the later M spectral types are observed to be more concentrated at the centre implies the presence of a metal abundance gradient in the bulge (Terndrup 1988; Blanco & Terndrup 1989), or a difference in mean age (mass).

5.3 Miras and other LPVs

There is evidence for a metallicity gradient in the data from the Mira variables. Whitelock et al. (1994) found a systematic change in the relative ratio of short period (more metal-poor) to long period (more metal-rich) Miras in bulge fields. The sense is that the ratio $R = P_{(200\text{-}300\mathrm{d})}/P_{(400\text{-}600\mathrm{d})}$ increases with distance from the Galactic Centre. The values observed by Whitelock et al. (1994) are $R = 1.1$, 1.8 and 3.9 for the fields at 2°.6, 4° and 7°.5, respectively.

5.4 The planetary nebulae

The kinematics of the planetary nebulae (PN) towards the Galactic bulge are discussed by Kinman, Feast & Lasker (1988). They find that the mean velocity increases away from the minor axis as $V_m = (12.0\ l - 13.6)$ km s^{-1} deg^{-1}, and the mean velocity dispersion $\sigma = 103$ km s^{-1}. These kinematics are similar to the kinematics of metal-rich bulge giants. The masses of these PN are consistent with old progenitors (Kinman et al. 1988). Acker et al. (1991) report that the mean velocity of planetary nebulae increases to 15 km s^{-1} deg^{-1} with distance from the Galactic Centre. These planetaries are located at the distance of the bulge (Stasinska et al. 1991), and their kinematics are consistent with the results of Kinman et al. (1988). In conclusion, the PN trace the kinematics of the metal-rich bulge.

There are contradictory data indicating different abundances for the bulge planetary nebulae. Ratag et al. (1992) find that the abundances for a large sample of bulge planetaries turn out to be much more metal-poor than the metallicities derived by Rich (1988) for K giants in Baade's window. However, the kinematics of the bulge planetary nebulae are consistent with bulge membership. This is puzzling because the metal abundances of the bulge planetaries suggested that they originated from the most metal-poor tail of the bulge stellar distribution, as did the RR Lyrae stars (e.g. Stasinska 1993; Renzini 1994). The new metallicities for bulge giants (McWilliam & Rich 1994; this work) shift the whole abundance scale to more metal-poor values, thus implying that the planetary nebulae do not originate only from the metal-poor bulge giants as do the RR Lyrae stars. Hence, the planetary nebulae now have metallicities and kinematics that are consistent with the bulk of the bulge population.

6 THE METALLICITY GRADIENT

Here we will discuss the metallicity gradient of the bulge, which is a crucial piece of evidence in favour of formation via dissipational collapse.

A metallicity gradient in the bulge fields along the minor axis was first observed by Terndrup (1988). The presence of a gradient is clear, as reviewed by Terndrup (1993), although not all the determinations agree with each other in the extent or even scale of the metallicity gradient. For example, Tyson

Table 4. Photometry and metallicities (field F588).

Star	R	R–I	B—R	Co	[Fe/H]	ST	Star	R	R–I	B—R	Co	[Fe/H]	ST
A-1	16.10	0.91	1.11	AR	-1.90	K	A-2	16.89	1.24	1.87	AR	-0.65	K
A-3	15.51	0.85	1.18	AR	-1.45	K	A-4	16.57	0.96	1.64	AR	0.05	K
A-5	16.55	0.97	1.30	AR	-1.55	K	A-6	16.53	0.95	1.48	AR	-0.35	K
A-7	16.82	1.08	1.82	AR	-1.05	K	A-8	16.36	0.85	1.44	AR	-1.15	K
A-9	15.82	1.25	1.83	AR	-0.25	M	A-10	16.84	0.90	1.27	AR	-0.85	K
A-11	16.81	1.00	1.82	AR	-1.05	K	A-12	16.40	0.91	1.23	AR	0.75	K
A-13	16.57	1.02	1.11	AR	-0.85	K	A-14	16.77	0.99	1.32	AR	-0.85	K
A-15	15.93	0.91	1.51	AR	-0.95	K	A-16	16.59	0.94	1.41	AR	-0.85	K
A-17	16.40	0.90	1.39	AR	-0.05	K	A-18	16.89	1.23	1.68	AR	0.25	K
A-19	16.79	1.10	1.84	AR	0.35	K	A-20	16.41	1.06	1.67	AR	0.25	K
A-21	16.64	0.86	1.45	AR	-0.55	K	A-22	16.76	1.02	1.80	AR	-0.25	K
A-23	15.78	0.95	1.87	AR	-0.55	K	A-24	16.76	0.93	1.70	AR	0.25	K
A-25	—	—	—	AR	...	M	A-25	16.64	1.04	1.88	AR	-0.35	K
A-26	16.89	1.24	1.87	AR	-0.55	K	A-27	16.64	0.97	1.35	AR	-0.75	K
A-28	16.45	0.89	1.59	AR	-0.55	K	A-29	16.73	0.90	1.41	AR	0.05	K
A-31	16.80	1.07	1.29	AR	-1.90	K	A-32	15.73	0.88	1.41	AR	-1.35	K
A-33	15.84	1.19	1.94	AR	-0.15	K	A-34	16.61	0.89	1.14	AR	-1.45	K
A-35	16.31	0.93	1.47	AR	-0.95	K	A-36	16.87	1.03	1.30	AR	-0.35	K
A-37	15.99	1.04	1.81	AR	-0.25	K	A-38	16.61	1.05	1.76	AR	-0.95	K
A-39	16.49	0.89	1.27	AR	0.45	K	A-40	15.66	1.05	1.61	AR	-1.45	K
A-41	16.70	0.86	1.62	AR	0.35	K	A-42	16.43	0.97	1.40	AR	-0.15	K
A-43	16.63	0.87	1.27	AR	0.65	K	A-44	16.62	1.05	1.44	AR	0.05	K
A-45	16.74	1.00	1.34	AR	0.05	K	A-46	16.76	1.02	1.80	AR	0.65	K
A-47	15.56	1.06	1.85	AR	-0.95	K	A-48	15.63	0.90	1.31	AR	-0.15	K
A-49	16.07	0.99	1.61	AR	0.05	K	A-50	15.52	1.04	1.83	AR	-0.65	K
A-51	16.65	1.06	1.34	AR	0.45	K	A-52	16.65	0.89	1.31	AR	-0.25	K
A-53	16.61	1.07	1.64	AR	-0.55	K	A-55	16.75	0.89	1.55	AR	-0.45	K
A-56	15.76	1.00	1.64	AR	-1.25	K	A-57	16.86	0.98	1.65	AR	0.45	K
A-58	15.98	0.96	1.16	AR	-1.55	K	A-59	16.74	0.89	1.25	AR	-1.05	K
A-60	16.90	1.12	1.33	AR	-0.45	K	A-61	16.38	0.95	1.15	AR	0.75	K
A-62	15.89	1.08	1.83	AR	-0.35	K	A-63	16.09	1.02	1.84	AR	-0.45	K
A-64	16.13	1.17	1.92	AR	-0.15	K	A-65	15.86	1.27	1.56	AR	0.35	K
A-66	16.50	1.09	1.46	AR	0.65	K	A-67	16.58	0.96	1.79	AR	-0.85	K
A-68	16.23	1.28	1.57	AR	-0.45	K	A-69	16.08	1.00	1.69	AR	-0.45	K
A-70	16.32	1.03	1.80	AR	-0.65	K	A-71	15.85	0.99	1.82	AR	-1.15	K
A-72	16.64	0.93	1.76	AR	0.45	K	A-25	—	—	—	AR	...	M
A-26	—	—	—	AR	...	K	A-73	16.70	0.98	1.63	AR	-1.90	K
A-74	15.52	1.04	1.83	AR	-0.55	K	A-75	15.99	1.04	1.34	AR	-1.55	K
A-76	15.72	0.94	1.53	AR	0.45	K	A-77	16.38	1.06	1.87	AR	-1.15	K
A-78	16.73	1.11	1.70	AR	-1.55	K	A-79	16.97	1.04	1.53	AR	-0.45	K
A-80	16.03	1.14	1.43	AR	0.35	K	A-81	16.73	0.99	1.54	AR	-1.70	K
A-82	16.62	0.87	1.25	AR	-1.35	K	A-83	16.84	0.99	1.34	AR	-1.90	K
A-84	16.74	1.05	1.37	AR	0.15	K	A-85	16.06	1.16	1.87	AR	-0.15	K
A-86	16.37	1.43	1.96	AR	0.95	K	A-87	16.72	0.91	1.56	AR	-0.65	K
A-88	16.68	0.90	1.84	AR	-0.25	K	A-89	15.82	1.00	1.11	AR	-0.35	K
A-90	16.55	0.99	1.76	AR	-0.25	K	A-91	16.58	0.96	1.79	AR	-0.75	K
A-92	16.20	0.96	1.55	AR	0.35	K	A-93	16.06	1.26	1.97	AR	-0.15	K
A-94	16.57	0.97	1.80	AR	-0.45	K	A-95	15.84	0.88	1.26	AR	0.15	K
A-96	16.42	0.87	1.61	AR	0.35	K	A-25	—	—	—	AR	...	K
A-97	15.97	0.99	1.89	AR	-1.90	K	A-98	16.64	1.06	1.62	AR	-1.35	K
A-99	16.67	0.98	1.81	AR	-1.15	K	A-100	16.38	0.95	1.35	AR	-0.15	K
A-101	16.65	0.91	1.48	AR	-0.05	K	A-102	16.03	1.12	1.75	AR	-1.90	K
A-103	16.17	1.02	1.75	AR	-0.25	K	A-104	15.53	1.55	1.71	AR	-0.45	K
A-105	16.68	1.06	1.20	AR	-1.90	K	A-106	16.85	1.33	1.80	AR	-1.25	K
A-107	17.00	1.13	1.24	AR	-1.55	K	A-108	16.58	1.10	2.03	AR	-0.75	K
A-109	16.70	1.01	1.47	AR	1.15	K	A-110	15.72	1.31	2.06	AR	-0.65	K
A-111	15.70	0.85	1.36	AR	-1.05	K	A-112	16.69	0.95	1.86	AR	0.05	K
A-113	16.14	1.08	1.78	AR	-0.05	K	A-114	16.63	0.94	1.23	AR	0.35	K
A-115	16.40	0.99	1.50	AR	-0.05	K	A-116	16.34	1.11	1.73	AR	-0.55	K

Table 4 – *continued*

Star	R	R–I	B—R	Co	[Fe/H]	ST	Star	R	R–I	B—R	Co	[Fe/H]	ST
A-117	16.20	0.92	1.22	AR	-1.05	K	A-118	16.38	0.90	1.13	AR	0.65	K
A-119	16.72	0.94	1.30	AR	1.15	K	A-120	16.65	0.89	1.77	AR	-0.55	K
B-1	16.34	0.91	1.57	AR	-0.95	K	B-2	16.12	1.15	1.25	AR	-0.25	K
B-3	16.98	1.10	1.84	AR	-0.45	K	B-4	16.63	1.13	1.69	AR	0.45	K
B-5	16.89	0.99	1.37	AR	0.65	K	B-6	16.84	1.01	1.47	AR	0.65	K
B-7	16.78	0.96	1.52	AR	-0.35	K	B-8	16.64	1.02	1.57	AR	-0.75	K
B-9	15.95	0.94	1.64	AR	-0.85	K	B-10	16.65	0.89	1.31	AR	-0.15	K
B-11	16.77	1.17	1.64	AR	0.35	K	B-12	16.82	1.06	1.43	AR	0.25	K
B-13	16.76	0.93	1.38	AR	0.55	K	B-14	15.84	0.88	1.26	AR	0.35	K
B-15	16.76	0.93	1.70	AR	0.25	K	B-16	15.76	1.72	2.07	AR	-0.55	M
B-17	16.64	1.03	1.19	AR	0.65	K	B-18	16.70	0.89	1.56	AR	-1.90	K
B-19	16.80	0.86	1.11	AR	0.45	K	B-20	16.68	1.03	1.67	AR	0.15	K
B-21	16.33	0.92	1.34	AR	-0.45	K	B-22	16.56	0.93	1.17	AR	0.85	K
B-23	16.21	1.05	1.52	AR	-0.15	K	B-24	16.86	1.01	1.53	AR	-0.75	K
B-25	16.90	1.04	1.72	AR	-0.15	K	B-26	15.65	1.88	2.13	AR	-0.55	M
B-27	16.46	0.87	1.19	AR	-0.55	K	B-28	16.25	0.91	1.12	AR	-1.55	K
B-29	16.88	0.97	1.79	AR	0.35	K	B-30	16.84	1.01	1.47	AR	1.15	K
B-31	15.87	1.11	1.47	AR	-0.35	K	B-32	16.41	0.97	1.69	AR	-0.35	K
B-33	16.77	1.06	1.17	AR	0.25	K	B-34	15.85	1.40	1.75	AR	-0.15	M
B-35	15.89	1.06	1.98	AR	0.25	K	B-36	16.33	1.16	1.87	AR	0.05	K
B-37	16.64	0.89	1.14	AR	-0.95	K	B-38	15.84	0.88	1.26	AR	-0.25	K
B-39	16.02	1.33	2.15	AR	-0.45	M	B-40	15.85	0.88	1.56	AR	-0.75	K
B-41	16.45	0.89	1.14	AR	-0.05	K	B-42	16.44	0.91	1.21	AR	-0.55	K
B-43	16.27	0.92	1.66	AR	-0.45	K	B-44	16.52	0.98	1.27	AR	1.05	K
B-45	16.54	0.88	1.16	AR	0.45	K	B-46	16.86	0.92	1.45	AR	-0.25	K
B-47	16.67	0.89	1.12	AR	0.75	K	B-48	15.61	0.90	1.24	AR	0.05	K
B-49	16.73	0.97	1.56	AR	0.35	K	B-50	16.96	1.16	1.82	AR	-0.55	K
B-51	16.37	0.91	1.42	AR	-1.55	K	B-52	16.10	0.86	1.62	AR	-1.35	K
B-53	16.22	1.47	1.90	AR	-0.15	M	B-54	16.65	1.11	1.58	AR	0.65	K
B-55	16.40	0.97	1.31	AR	-1.05	K	B-56	16.92	1.01	1.64	AR	-0.75	K
B-57	16.82	1.10	1.43	AR	-0.15	K	B-58	16.36	0.98	1.27	AR	0.35	K
B-60	15.52	1.04	1.83	AR	-0.85	K	B-61	16.03	1.12	1.79	AR	-0.05	K
B-62	16.65	0.89	1.77	AR	0.05	K	B-63	16.02	1.33	2.15	AR	1.15	M
B-64	16.62	0.87	1.50	AR	0.35	K	B-65	16.75	0.96	1.61	AR	0.15	K
B-66	15.87	0.87	1.19	AR	-1.55	K	B-67	16.95	1.04	1.18	AR	0.75	K
B-68	16.56	0.96	1.63	AR	0.25	K	B-69	16.62	0.93	1.31	AR	-0.85	K
B-70	16.76	0.91	1.37	AR	-1.55	K	B-71	15.95	1.16	1.28	AR	-1.90	K
B-72	16.81	1.08	1.99	AR	-0.05	K	B-73	16.21	1.38	1.55	AR	1.15	M
B-74	16.82	1.03	2.10	AR	0.05	K	B-75	16.55	1.58	1.67	AR	0.25	K
B-76	16.02	0.98	1.67	AR	-0.05	K	B-77	16.04	1.06	1.59	AR	-0.95	K
B-78	16.65	1.11	1.58	AR	0.45	K	B-79	16.69	0.89	1.13	AR	0.05	M
B-80	16.66	0.93	1.54	AR	-0.15	K	B-81	16.91	1.14	1.50	AR	-0.75	K
B-82	16.83	0.96	1.80	AR	-0.45	K	B-83	16.27	1.56	1.33	AR	-1.90	M
B-84	16.89	1.24	1.87	AR	-0.95	K	B-85	16.44	0.90	1.11	AR	0.65	K
B-86	15.63	0.90	1.31	AR	-1.05	K	B-87	15.50	1.14	1.82	AR	-0.75	K
B-88	16.45	0.93	1.37	AR	-0.70	K	B-89	16.63	1.01	1.57	AR	-0.95	K
B-90	16.46	0.97	1.11	AR	0.05	K	B-91	15.88	0.93	1.53	AR	0.15	K
B-92	16.53	0.88	1.37	AR	0.15	K	B-93	15.95	1.02	1.98	AR	-0.95	K
B-94	15.93	1.29	1.54	AR	-0.05	K	B-95	16.21	1.05	1.48	AR	0.05	K
B-96	15.94	1.79	2.28	AR	-0.15	M	B-97	16.18	1.26	1.98	AR	0.65	K
B-98	16.53	1.00	1.63	AR	0.15	K	B-99	16.70	1.13	1.33	AR	-1.90	K
B-100	16.37	0.99	1.20	AR	-0.15	K	B-101	16.51	0.97	1.32	AR	-0.55	K
B-102	16.87	1.04	1.43	AR	0.55	K	B-103	16.69	0.89	1.13	AR	-1.25	K
B-104	17.06	1.13	1.99	AR	-0.65	K	B-105	15.64	1.14	1.55	AR	0.25	K
B-106	16.35	1.79	1.45	AR	1.05	M	B-107	16.12	0.95	1.57	AR	-1.90	K
B-108	16.65	0.87	1.21	AR	-0.75	K	B-109	15.86	1.16	2.13	AR	-0.15	K
B-110	16.42	0.87	1.61	AR	-0.55	K	B-111	15.50	1.14	1.82	AR	-0.85	K
B-112	16.01	0.87	1.52	AR	-0.65	K	B-113	15.95	1.23	1.80	AR	-0.35	K
B-114	15.56	1.70	1.98	AR	-0.75	M	B-115	16.85	0.94	1.39	AR	0.15	K

Table 4 – *continued*

Star	R	R–I	B—R	Co	[Fe/H]	ST	Star	R	R–I	B—R	Co	[Fe/H]	ST
B-116	16.47	0.89	1.88	AR	0.15	K	B-117	16.24	1.02	1.91	AR	-0.05	K
B-118	16.63	0.86	1.18	AR	-1.25	K	B-119	16.71	0.96	1.47	AR	0.25	K
B-120	16.94	1.05	1.66	AR	-0.05	K	13-06	16.02	1.20	1.44	MX	-0.05	K
13-18	13.97	1.27	1.93	MX	-0.65	M?	13-20	15.42	0.93	1.36	MX	0.35	K
13-25	15.46	0.91	2.19	MX	-1.35	K	13-26	14.75	1.02	1.75	MX	-1.90	K
13-33	15.95	0.87	1.80	MX	-0.95	K	13-35	15.52	1.04	1.83	MX	-1.15	K
13-37	15.56	1.01	1.84	MX	-0.95	K	13-41	15.42	1.28	2.11	MX	-0.85	K
13-43	16.65	1.08	1.86	MX	0.05	K	13-47	15.53	1.12	1.90	MX	-0.45	K
13-48	15.77	0.84	1.63	MX	-0.75	K	13-50	15.12	0.92	1.60	MX	-0.25	K
13-52	14.16	0.81	2.09	MX	-1.45	K	13-59	15.86	1.16	2.13	MX	-0.75	K
61-08	14.63	1.01	1.01	MX	1.15	K	61-14	—	—	—	MX	...	K
61-20	16.13	0.85	1.41	MX	-0.05	K	61-21	15.89	1.00	1.31	MX	0.05	K
61-27	—	—	—	MX	...	K	61-28	16.33	1.16	1.87	MX	-0.55	K
61-32	14.62	0.02	1.45	MX	-1.45	K	61-35	16.44	1.00	1.59	MX	-1.05	K
61-37	15.87	1.32	1.08	MX	0.85	M?	61-39	16.22	1.10	2.09	MX	-1.15	K
61-40	16.52	1.01	1.95	MX	-1.70	K	61-43	16.01	2.27	1.59	MX	-1.15	K
61-45	16.02	1.07	1.93	MX	...	K	61-47	16.65	0.95	1.85	MX	-0.05	K
61-52	14.89	1.19	1.28	MX	-0.05	K	61-53	15.20	1.32	1.97	MX	-0.85	K
61-55	14.89	1.07	1.42	MX	-0.85	K	61-61	14.73	1.31	1.90	MX	-0.85	K
61-64	15.89	1.06	1.98	MX	-0.85	K	61-68	—	—	—	MX	...	K
9-09	16.65	0.95	1.75	MX	-0.55	K	9-10	—	—	—	MX	...	K
9-11	15.66	0.92	1.91	MX	-1.25	K	9-16	15.97	0.99	1.89	MX	-1.25	K
9-17	13.48	0.84	1.05	MX	-0.85	K	9-20	14.78	1.31	1.90	MX	-0.45	K
9-23	16.32	1.18	1.97	MX	-1.05	K	9-24	16.20	0.92	1.10	MX	-0.95	K
9-28	15.53	0.85	1.66	MX	-1.75	K	9-36	15.56	1.06	1.85	MX	-1.05	K
9-37	16.90	1.08	1.85	MX	-0.55	K	9-38	13.45	0.85	0.55	MX	1.15	K
9-39	15.49	1.10	1.44	MX	-1.05	K	9-41	14.57	1.25	1.88	MX	-0.55	K
9-43	15.68	1.22	1.35	MX	-1.90	K	9-45	15.95	1.32	1.45	MX	-0.45	K
9-46	15.71	0.92	2.26	MX	-1.70	K	9-48	15.62	1.14	1.82	MX	-1.90	K
9-50	16.23	1.09	1.56	MX	-1.90	K	9-51	16.70	1.11	1.60	MX	-0.95	K
9-57	15.64	1.18	1.66	MX	-1.55	K	9-60	15.67	1.14	1.28	MX	-1.55	K
9-64	16.02	1.33	2.25	MX	-0.85	M?	20-01	16.02	1.33	2.15	MM	-1.35	M
20-02	15.71	2.52	2.13	MM	-1.05	M	23-01	15.68	2.37	2.09	MM	-1.15	M
23-02	15.85	1.40	1.75	MM	-0.65	M	25-01	15.49	1.14	1.87	MM	-1.35	M
25-02	15.51	2.48	2.05	MM	-1.55	K	27-01	15.82	1.25	1.83	MM	-0.75	K
27-02	15.29	1.06	1.81	MM	-0.95	M	29-01	15.22	1.15	1.37	MM	-1.70	K
29-02	14.74	1.05	1.74	MM	-0.85	K	41-01	16.58	0.73	1.51	MM	-1.45	K
41-02	15.97	0.87	1.80	MM	-1.25	K	43-01	16.67	0.86	1.18	MM	0.65	M
43-02	—	—	—	MM	...	K	43-03	—	—	—	MM	...	K
45-01	16.62	1.14	1.55	MM	-1.55	K	45-02	—	—	—	MM	...	K
45-03	—	—	—	MM	...	K	47-01	—	—	—	MM	...	K
47-02	—	—	—	MM	...	K	129-01	15.36	1.17	2.15	MM	-1.35	K
129-02	15.50	1.14	1.82	MM	-1.90	K	131-01	—	—	—	MM	...	K
131-03	16.06	0.93	1.78	MM	-1.70	K	133-01	15.86	1.16	2.13	MM	-1.35	K
137-01	13.81	0.67	0.55	MM	1.15	K	139-01	16.22	3.04	2.23	MM	-1.55	K

Table 5. Photometry and metallicities (M22 field).

Star	V	B-V	[Fe/H]	ST	Star	V	B-V	[Fe/H]	ST
86	14.33	1.59	-1.90	K	408	15.13	1.29	-1.90	K
467	15.12	1.17	-1.90	K	681	14.69	1.56	-1.90	K
385	15.05	1.21	-1.90	K	386	14.23	0.89	-1.90	K
203	15.01	1.23	-1.90	K	510	14.16	1.38	-1.90	K
292	15.05	1.30	-1.55	K	383	15.08	1.59	-1.45	K
494	13.50	1.25	-1.45	K	500	13.60	1.65	-1.45	K
637	13.62	1.61	-1.35	K	41	14.38	1.52	-1.35	K
53	14.11	1.33	-1.35	K	392	13.62	1.80	-1.25	K
320	15.41	1.69	-1.25	K	315	14.97	1.53	-1.25	K
403	14.47	1.40	-1.25	K	411	14.64	1.61	-1.25	K
610	14.62	1.38	-1.15	K	578	14.24	1.48	-1.15	K
218	14.84	1.66	-1.15	K	571	15.49	1.36	-1.05	K
690	14.83	1.38	-1.05	K	703	15.34	1.55	-1.05	K
196	15.10	1.74	-0.95	K	511	14.88	1.68	-0.95	K
114	14.75	1.19	-0.95	K	314	14.79	1.46	-0.95	K
39	14.26	1.41	-0.85	K	567	15.17	1.33	-0.85	K
714	14.52	1.51	-0.75	K	18	14.50	1.54	-0.75	K
717	14.34	1.72	-0.65	K	6	14.09	1.41	-0.65	K
591	14.00	1.10	-0.65	K	307	14.89	1.45	-0.65	K
36	14.96	1.36	-0.65	K	303	14.82	1.59	-0.65	K
84	14.67	1.44	-0.65	K	721	14.23	1.37	-0.55	K
662	14.98	1.29	-0.55	K	726	14.43	1.31	-0.55	K
50	14.65	1.54	-0.55	K	719	14.33	1.52	-0.55	K
393	14.54	1.33	-0.45	K	140	14.98	1.41	-0.45	K
516	14.12	1.35	-0.35	K	607	14.68	1.37	-0.35	K
148	14.25	1.68	-0.35	K	101	14.27	1.52	-0.35	K
577	15.22	1.43	-0.35	K	689	15.10	1.54	-0.25	K
691	15.26	1.59	-0.25	K	13	15.20	1.52	-0.25	K
371	15.14	1.27	-0.15	K	7	14.73	1.49	-0.15	K

Table 5 – *continued*

Star	V	B-V	[Fe/H]	ST	Star	V	B-V	[Fe/H]	ST
156	14.44	1.56	-0.15	K	279	14.81	1.56	-0.15	K
52	14.70	1.49	-0.05	K	152	14.98	1.70	-0.05	K
308	14.71	1.54	-0.05	K	29	15.07	1.25	-0.05	K
211	14.31	1.51	0.20	K	522	15.24	1.37	0.20	K
328	15.33	1.45	0.20	K	618	14.24	1.38	0.20	K
231	14.26	1.64	0.20	K	687	14.53	1.01	0.20	K
402	14.92	1.50	0.20	K	318	14.94	1.36	0.20	K
300	14.98	1.20	0.20	K	139	15.13	1.39	0.20	K
40	15.15	1.29	0.20	K	588	14.59	0.97	0.20	K
425	15.13	1.59	0.20	K	58	14.51	1.17	0.20	K
275	14.90	1.45	-1.90	M	33	13.85	1.62	-0.65	M
36	13.80	1.70	-0.95	M	584	14.84	1.45	-1.90	M
575	15.06	1.78	-1.90	M	277	14.38	1.63	-0.95	M?
410	14.99	1.26	0.20	M	590	14.93	1.68	-0.35	M
161	14.90	1.57	0.20	M	41	13.48	2.02	-0.75	M
412	11.66	1.25	0.20	K	373	14.60	1.64	0.20	M?
515	13.49	2.00	-0.85	K	494	13.50	1.25	-1.45	K
500	13.60	1.65	-1.45	K	392	13.62	1.80	-1.25	K
637	13.62	1.61	-1.35	K	19	13.77	1.91	-0.95	K
424	13.81	1.71	-0.05	K	61	13.94	1.93	-0.55	K
426	13.98	1.18	-0.45	K	27	13.98	1.18	0.20	K
478	14.47	1.09	-1.90	2	274	14.75	0.23	0.20	2HB
215	12.47	1.43	-1.90	2	12	14.10	0.60	0.20	2HB
720	13.72	1.13	-1.90	2	574	14.45	0.42	0.20	2HB
85	14.06	1.13	-1.90	2	55	13.12	1.27	-1.90	2
367	13.79	1.03	0.20	2	555	12.17	1.36	0.20	2
572	0.00	0.00	0.20	2	42	00.00	0.00	-1.90	2

Notes to table: K = K giant, M = M giant, 2 = M22 member, 2HB = M22 Horizontal Branch star.

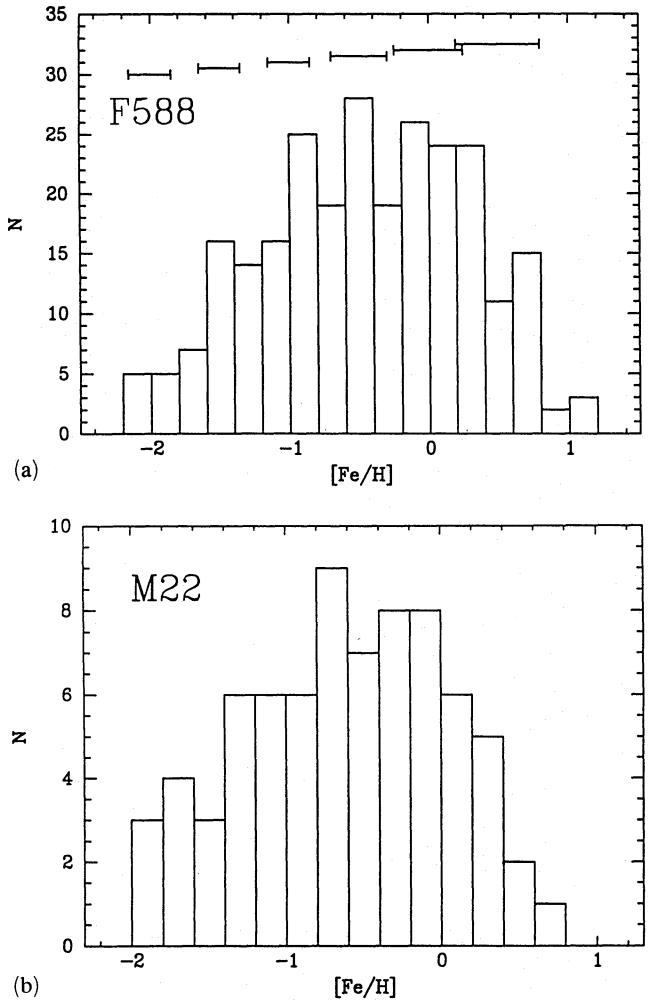

Figure 3. (a) Metallicity distribution for the K giants observed in F588. The 2σ error bars of the abundances are shown. All abundances higher than [Fe/H] ~ +0.5 are extrapolations. (b) Metallicity distribution for all the bulge giants measured in the field of M22. Error bars are the same as in (a).

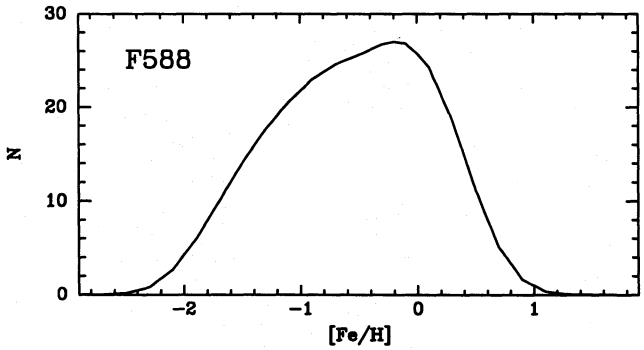

Figure 4. Metallicity distribution in field F588 obtained by Lucy deconvolution using the estimated errors.

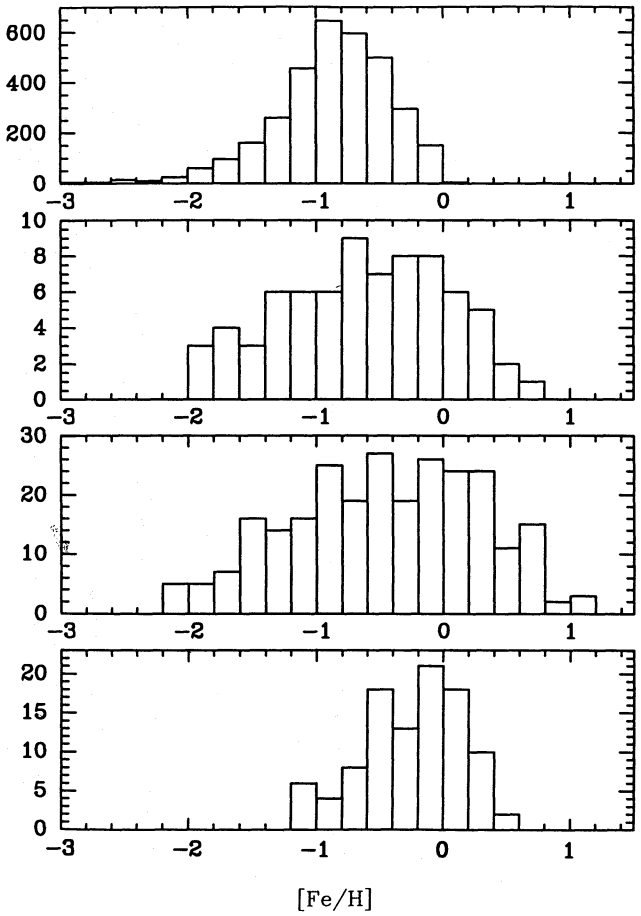

Figure 5. Metallicity distribution of different bulge fields. From bottom to top, the fields plotted are BW (from McWilliam & Rich 1994), F588 (this work), FM22 (this work) and MH (from Morrison & Harding 1993). This figure shows the large abundance spread at all distances and the metal abundance gradient.

& Rich (1993) find no metallicity gradient inside 1 kpc, and argue that the bulge formed via a dissipationless collapse. Table 6 presents all the determinations of the metal abundance in bulge fields. Essentially, four techniques have been used: *BVI* photometry (Cook 1987; Terndrup 1988), *JHK* photometry (Frogel et al. 1990; Minniti, Olszewski & Rieke 1995), Washington photometry (Tyson 1991; Geisler & Friel 1992; Morrison & Harding 1993) and spectroscopy [Rich 1988; Frogel et al. 1990; Terndrup et al. 1990; Smith & Plez 1993 (private communication); McWilliam & Rich 1994; this work]. The mean abundances obtained in these studies are plotted as a function of Galactocentric distance in Fig. 6. This figure shows a clear gradient, but note that at any given distance, the scatter in these mean abundances is very large. Unfortunately, it is difficult to assign relative weights to these different results.

The most reliable of these techniques should be spectroscopy. However, note that the high-dispersion echelle spectra analysed with model atmospheres give a mean metallicity [Fe/H] = −0.25 for BW (McWilliam & Rich 1994), which is more metal-poor than previous determinations. We will adopt this recent metallicity determination for the K giants in Baade's window.

This new more metal-poor scale is also supported by high-dispersion spectroscopy of M giants in Baade's window, which should represent the highest metallicity part of the population. Smith & Plez (1993) find a mean metallicity

Table 6. Metallicity determinations in the bulge fields.

Field	l	b	[Fe/H][1]	r[2]	Method	Reference
Sgr3	0°	−3°	+0.10	0.42	CMT1T2	Tyson (1991, 1993)
BW	1°	−4°	+0.00	0.56	BVI	Terndrup 1988
BW	1°	−4°	+0.39	0.56	CMT1T2	Tyson (1991, 1993)
BW	1°	−4°	+0.30	0.56	Spectra	Rich 1988
BW	1°	−4°	−0.25	0.56	Spectra	McWilliam + Rich 1994
BW	1°	−4°	0.00	0.56	Spectra	Smith + Plez 1993 [3]
6deg	0°	−6°	−0.20	0.84	BVI	Terndrup 1988
6deg	0°	−6°	+0.74	0.84	CMT1T2	Tyson (1991, 1993)
8deg	0°	−8°	−0.40	1.11	BVI	Terndrup 1988
8deg	0°	−8°	+0.07	1.11	CMT1T2	Tyson (1991, 1993)
10deg	0°	−10°	−0.70	1.39	BVI	Terndrup 1988
10deg	0°	−10°	+0.20	1.39	CMT1T2	Tyson (1991, 1993)
BW	1°	−4°	+0.20	0.56	CMT1T2	Geisler + Friel 1992
MH10deg	−10°	−10°	−0.80	1.69	CMT1T2	Morrison + Harding 1993
13deg	0°	−13°	−0.62	1.80	CMT1T2	Tyson (1991, 1993)
17deg	0°	−17°	−1.07	2.38	CMT1T2	Tyson (1991, 1993)
F588	8°	7°	−0.60	1.25	Spectra	This work
M22	10°	−7°	−0.60	1.43	Spectra	This work

Notes.
[1]Mean metallicities.
[2]Equivalent distances in kpc along the minor axis for a flattened bulge ($c/a = 0.7$).
[3]M giants only.

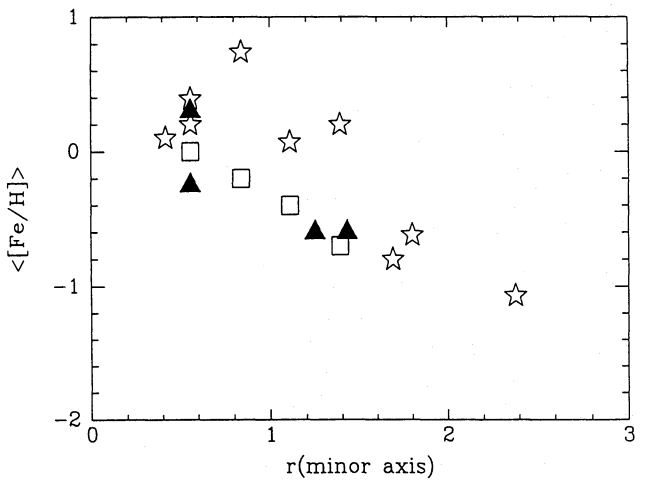

Figure 6. Mean metallicities published for bulge fields. Open squares are from Terndrup (1988) *BVI* photometry. Stars are the Washington photometry of Tyson (1993), Geisler & Friel (1992) and Morrison & Harding (1993). The filled triangles represent the spectroscopic determinations from Rich (1988), McWilliam & Rich (1994) and this work.

[Fe/H] = 0 for M giants, with a total range from about −0.1 to about 0.25. This is also significantly more metal-poor than the previous determinations of M giant abundances in BW by Terndrup et al. (1991), who found mean [M/H] = +0.3.

We have obtained metallicities of K giants based on medium dispersion spectra, calibrated solely on the scale of the globular clusters. Although the highest metallicity bins are not well defined, the mean abundance in field F588 at $(l, b) = (8°, 7°)$ is [Fe/H] = −0.55. This is the mean abundance of bulge + halo + disc giants present in the field, which is nonetheless dominated by bulge giants (Minniti 1995c). The same is the case for BW. Field F589 at $(l, b) = (12°, 3°)$ is complicated by the presence of substantial numbers of disc giants, therefore it does not give any useful metallicity information. Selection effects in the M22 field at $(l, b) = (-9.^{\circ}9, 7.^{\circ}6)$ might work against the inclusion of metal-rich bulge giants. Therefore, it only gives a lower limit for the mean metallicity, [Fe/H] ≥ −0.60. If we project the F588 and M22 fields to the minor axis, taking into account the flattening of the bulge $\varepsilon = 0.3$, they would correspond to $b = 10°$ and 12°, respectively. Thus, from spectroscopy we find a gradient $\mathrm{d[Fe/H]/d}r = 0.05$ dex deg^{-1} along the minor axis.

However, the question that is still open is whether this gradient is real or merely due to a population transition (different relative contributions of bulge and halo stars with distance from the centre). For example, one can interpret the metallicity distributions in different fields as the sum of two components that change their relative contributions with distance from the Galactic Centre (a metal-poor halo with mean [Fe/H] = −1.5, and a metal-rich bulge with mean [Fe/H] = 0.0). Discounting the stars with [Fe/H] ≤ −1 at BW, which are mostly halo giants on kinematic grounds (Minniti 1995c), we find a mean metallicity for the bulge itself of [Fe/H] = −0.1 at BW from the data of McWilliam & Rich (1994). Discounting the halo giants in our fields F588 and M22, we find a mean metallicity of [Fe/H] ≈ −0.3 for these fields. In consequence, the gradient in the bulge itself is somewhat shallower. However, this result depends on the adopted decomposition between bulge and halo, and a zero gradient for the bulge itself cannot be discarded.

The metallicity gradient can be interpreted as a gradient within the bulge component, although it may also be possible to model it gradient by a change in population mixes, in which each individual population does not have an spatial metallicity gradient. Again, there are also different selection effects in the photometric selection of the spectroscopic samples in all the fields that were used to compute this gradient. However, the mean abundance in a given field is unlikely to be affected significantly by the selection effects; systematic errors in the metallicity scales are much more

important. Clearly, more work is needed on this particular issue, because the absolute spectroscopic abundance scales are not very well defined yet.

The situation is not better for the photometric metallicities. Terndrup (1988) inferred a gradient $d[Fe/H]/dr = 0.12$ dex deg^{-1}, from the colour of the bulge red giant branch in optical bands. The spectroscopy of Terndrup et al. (1990) confirms that the TiO bands are stronger in M giants that are closer to the Galactic Centre, finding $d[Fe/H]/dr \approx 0.05$ dex deg^{-1}. Frogel et al. (1990) find similar behaviour for the CO bands.

Minniti et al. (1995) make a comparative study between the globular clusters and the bulge stellar population, using IR photometry in selected fields located at a few arcmin away from the cluster cores. Their major conclusion is that the bulge giants have the same near-IR colours in the mean as the most metal-rich globulars. They also find a metallicity gradient $d[Fe/H]/dr \approx 0.1$ dex deg^{-1}, confirming the results of Terndrup (1988). These abundances are based on the mean location of the bulge RGB using globular clusters as reference.

The Washington photometric system (defined by Canterna 1976) was used by Geisler & Friel (1990), Tyson (1991) and Morrison & Harding (1993) to derive abundances of bulge giants in different fields. They all obtained metallicities using the calibration of Geisler, Claria & Minniti (1991), and so their relative abundances should be on the same system. However, there are many difficulties for the photometry in these crowded bulge fields, added to the intrinsic problems with the calibrations (see Twarog & Anthony-Twarog 1994). Tyson (1991) and Geisler & Friel (1990) obtain the same mean metallicity for BW, which is about 0.5 dex higher than the mean metallicity derived by McWilliam & Rich (1994). The field of Morrison & Harding (1993) at $(l, b) = (-10°, -10°)$ would lie at a projected latitude $b \approx 13°$ accounting for the flattening of the bulge. They find a mean metallicity $[Fe/H] = -0.8$. A very steep gradient in metallicity of $d[Fe/H]/dr = 0.18$ dex deg^{-1} results from these observations.

However, Tyson (1991) scaled his metallicities upward to match the abundances of Rich (1988) in Baade's window. Otherwise, he would have obtained the same abundances as McWilliam & Rich (1994) in the BW field. In this latter – more accurate – scale, the photometry of Tyson (1991) predicts $[Fe/H] \approx -1.35$ at $b = 13°$, which differs by 0.5 dex from the mean abundances of Morrison & Harding (1993).

Tyson (1992; see also Rich 1993b) argues that the mean metallicity is constant within 1 kpc from the Galactic Centre, contradicting the results of Terndrup (1988) and Terndrup et al. (1990). If true, this is important because it would suggest a dissipationless collapse formation for the bulge, contrary to the kinematic arguments (Minniti 1995c). However, the proof that [Fe/H] decreases away from the centre is clearly seen by comparing the colour–magnitude diagrams of Udalski et al. (1993) at BW (at 0.5 kpc) with the fields at $(l, b) = (\pm 5°, 3°)$ (0.8 kpc), and at $-8°$ (1 kpc), or the colour–magnitude diagrams of Ortolani & Rich (1993; shown by Renzini 1993) at BW with the $-8°$ field, and the SgrI field at $-3°$ (shown by Rich 1993a). The inner fields show larger numbers of fainter and redder giants than the outer fields, as expected if the inner fields are more metal-rich, according to the findings of Bica et al. (1991). We note that metallicity has a far more important effect than age in determining this morphology of the red giant and horizontal branches.

To summarize, the abundances determined from photometry in bulge fields depend on the absolute calibrations to an uncertain degree, although the presence of a radial gradient seems well established for the whole population bulge plus halo plus disc. The most visually compelling proof for the existence of a metallicity gradient within the inner 1 kpc is given by the CMDs of Udalski et al. (1993).

7 THE ABSOLUTE METALLICITY OF THE GALACTIC BULGE

Early studies recognized that the bulge would be very metal-rich. Whitford (1978) noticed that the intense absorption lines seen in the integrated spectrum of the bulge were similar to those of giant elliptical galaxies. Rich (1988) determined the metallicity of 88 K giants in Baade's window, concluding that the mean metallicity was very high, $[Fe/H] = +0.3$. Such a value was supported by Washington photometry (Geisler & Friel 1990; Tyson 1991), and by infrared spectroscopy (Terndrup, Frogel & Whitford 1991). This implied that the bulge could be relatively young, since the turn-off of a metal-rich population with a certain age is redder than that of a metal-poor population. For example, Holtzmann et al. (1993) find an age of less than 10 Gyr assuming $[Fe/H] = +0.3$. Such extreme metallicity led to uncomfortable situations, like the very high Helium abundance expected for metal-rich stars: for the highest metallicity stars of Rich (1988) with $[Fe/H] \approx +1$, the stars are almost completely made of elements that are heavier than Hydrogen (e.g. Renzini 1992). Even worse, there are elliptical galaxies with much stronger lines, more metal-rich than the Milky Way bulge. Such a high bulge metallicity also led to speculations about a very different stellar evolution in the bulge, with the development of unusual phases of evolution for super metal-rich stars (e.g. Horch, Demarque & Pinsonneault 1992). It was also argued that perhaps metal-rich stars do not undergo the planetary nebula phase (e.g. Ratag et al. 1992; Stasinska 1993), and emit substantial far-UV radiation as AGB-manqué (Greggio & Renzini 1990).

However, careful analysis and modelling of echelle spectra revealed that the bulge giants in Baade's window are not so metal-rich (McWilliam & Rich 1994; Smith & Plez 1993). The mean metallicity of the bulge is less than solar, with some element ratios enhanced with respect to the solar value, indicating a different chemical evolution. Our analysis of giants in two fields further away from the Galactic Centre supports the idea that the bulge is not super metal-rich. In fact, in these regions the bulge may even be more metal-poor than the disc in situ (e.g. Balcells & Peletier 1994), even though McWilliam & Rich (1994) argued for a zero metallicity gradient in the disc based solely on the Baade's window data. This is a very important point for the study of the formation of different Galactic components. If the bulge is more metal-poor than the disc in these regions, it is likely that the bulge was formed before the underlying disc, unless strong infall of low metallicity gas occurred in the inner Galaxy at later epochs.

Unfortunately, one cannot make a detailed separation between individual bulge and disc stars in these low-latitude fields. What is done is to compare the mean abundance

observed in bulge fields with the expected mean abundance of the disc extrapolated towards the inner regions. There is a well-known metallicity gradient observed in the disc of the Galaxy (e.g. Janes 1978; Shaver et al. 1983). Although these measurements do not extend into the inner few kiloparsecs of the Galaxy, comparison with other spirals makes us suspect that this gradient must continue or at least flatten inside. Just as an example, a strong metallicity gradient that continues all the way to the centre is observed in the thoroughly studied nearby galaxies M33, M81 and M101 (Pagel & Edmunds 1981; Henry & Howards 1995). The presence of a bar in our Galaxy would favour a shallow inner metallicity gradient if the Milky Way behaves as other barred galaxies (Martin & Roy 1994; Zaritsky et al. 1994). In any case, the mean metallicity of the bulge, at about 1.5 kpc from the Galactic Centre, is significantly *lower* than the mean metallicity in the solar neighbourhood. Therefore, we conclude that the bulge is more metal-poor than the disc in situ. As emphasized by Balcells & Peletier (1994), the Galactic bulge is not super metal-rich.

8 CHEMICAL EVOLUTION OF THE BULGE

An important piece of evidence to decide about bulge formation is given by the detailed chemical evolution of the bulge. Here we will briefly summarize what is known about this subject, along the lines of Wyse & Gilmore (1992). The ejecta from massive stars that undergo supernova (SN) Type II explosions are rich in oxygen, α elements (Mg, Si, Ca, Ti), and *r*-process elements with respect to elements of the iron peak (Fe, Cr, Mn, Sc, V, etc.). On the other hand, the explosions from SN Type I produce more heavy elements with respect to light elements (e.g. Arnett 1978; Spite & Spite 1985; Wheeler, Sneden & Truran 1989; Nomoto, Thielemann & Yokoi 1984; Thielemann, Nomoto & Hashimoto 1990; Wyse & Gilmore 1992).

The halo stars have oxygen and α elements enhanced with respect to iron due to enrichment by SN Type II only (e.g. Wheeler et al. 1989). Since the formation of the halo was slow and chaotic (e.g. Searle & Zinn 1978), the bulge gas had the opportunity to be enriched by the ejecta from SN Type I, resulting in gas compositions with [O/Fe] and $[\alpha/\mathrm{Fe}] \sim 0$. If the bulge star formation took place rapidly (e.g. Matteucci & Brocatto 1990), then bulge SN Type II would have been important in driving the O and α element abundance up again. We would then expect [O/Fe] and $[\alpha/\mathrm{Fe}] \geq 0$, consistent with the results of McWilliam & Rich (1994; also Barbuy & Grenon 1990). However, if the formation of the bulge was slow, the iron peak elements would dominate ([O/Fe] and $[\alpha/\mathrm{Fe}] \leq 0$), contrary to the observations.

The real test, however, will be given by the measurement of detailed abundances for large numbes of giants spanning the whole abundance range found in bulge fields. The available data (McWilliam & Rich 1994; Wheeler et al. 1989; Edvarsson et al. 1993), suggest that the chemical evolution of the bulge is also different from that of the local disc and the local halo. In particular, at a given [Fe/H], the bulge giants have higher [Al/Fe], [Mg/Fe] and [Ti/Fe] than the disc giants. The presence of enhanced Eu abundance also suggests that the SN Type II played an important role in the enrichment of the bulge, unlike the disc. Interestingly, the metal-rich globular cluster M71 and the bulge giants seem to share similar detailed chemical composition, suggesting similar chemical evolution (Sneden et al. 1994).

The He abundance for different bulge fields was recently measured by Minniti (1995b) using the R method (Iben 1968; Buzzoni et al. 1983). The mean He abundance of the bulge is $Y = 0.28 \pm 0.02$, consistent with a moderate metallicity, and not with super metal-rich populations, where one expects $Y \geq 0.3$–0.35 (e.g. Renzini 1994). The bulge He abundance is similar to those of the metal-rich globular clusters (Minniti 1995b). Also, there is no indication of a significant gradient in Y.

9 IMPLICATIONS FOR THE FORMATION OF THE BULGE

If we knew the formation history of the early Galactic components, we could then have a clearer understanding of the cosmological Universe. Obviously, if the bulge formed very rapidly (e.g. Matteucci & Brocatto 1990), and if it is relatively young ($t \leq 10$ Gyr), the observable Universe would be plagued with forming bulges. On the other hand, if the bulge is the result of several accretion processes within the age of the Galaxy, we should observe a significant range in ages (and therefore carbon stars) in the bulge population.

Hartwick (1976) concludes that the abundance distribution of the globular clusters and halo is explained if most of the gas (~ 90 per cent) was suddenly lost from the halo. Recently, Carney et al. (1990) pointed out a very simple but important fact: the gas left over from the Galactic halo formation would have sunk to the bulge, rather than to the disc, owing to its low angular momentum. The alternative would be that the gas could be blown away by supernovae winds. This possibility is important in lower mass galaxies, but the Milky Way is massive enough that it should have retained a significant fraction of the gas. This was appreciated by Wyse & Gilmore (1992, 1993), who reviewed several alternatives for bulge formation. They preferred the idea that the halo formed first, preceding the bulge, based largely on Carney et al. (1990). In this scenario there is a causal relation between the halo and bulge.

One of the most important observable signatures of dissipation during the formation is the presence of a metallicity gradient, as discussed by ELS, Larson (1976) and Carlberg (1984). Even though metallicity gradients can also arise in other formation processes, the strong observed correlation between kinematics and metallicity (Minniti 1995c) also favours dissipation. Further work along these lines would be to determine the difference – if any – between a radial and vertical metallicity gradient in the bulge, in order to compare with specific predictions from numerical models like those of Pfenniger & Norman (1990), Sellwood (1993) and Friedli et al. (1994).

10 CONCLUSIONS

We have measured metallicities for large samples of K giants in two Galactic bulge fields at 1.5 and 1.7 kpc projected distance from the Galactic Centre.

The mean metallicity at these distances, $[\mathrm{Fe/H}] = -0.6$, is lower than that of the K giants in Baade's window. Thus, there is a metal abundance gradient in the inner 2 kpc,

confirming the results from previous photometric observations. This could be because of the interplay of different Galactic components (i.e. bulge versus halo) or intrinsic to the bulge itself. Since the mean metallicity of the bulge is less than Solar ([Fe/H]≤0), we argue that the underlying disc could be more metal-rich than the bulge itself.

The selection of candidates for both fields was different, as described in Section 2. However, the results (metallicity distributions and mean abundances) seem to be consistent for both fields, located at similar distances from the Galactic Centre, but in opposite sides of the Galactic plane, which is encouraging.

Our best estimate for the metallicity distribution of giants at 1.5 kpc from the Galactic Centre is given, after deconvolving the observational errors (Fig. 4). From this we conclude that a large abundance spread is seen, in agreement with the large abundance spread seen in the Baade's window. This spread is beyond that predicted by the observational scatter alone. The large metallicity range seen in different bulge fields should be taken into account when deriving the ages of its constituent populations. The combinations of different metallicities and ages could conspire to give a narrow MS turn-off, such as that found by Holtzmann et al. (1993). For example, there are possible combinations of an old, metal-poor population superimposed on a younger, metal-rich population, for which the CMDs at the main sequence turn-off would not look much wider.

The presence of a metallicity gradient, combined with a clear correlation between metal abundance and kinematics of stars in the Galactic bulge, indicate that the inner portions of the Galaxy show the signature of dissipation. However, the alternative interpretation that the gradient itself is caused by the mixing of different components in the inner Galaxy cannot be ruled out.

ACKNOWLEDGMENTS

We thank N. Suntzeff for help at the telescope and advice during the reductions. We also thank D. Terndrup (the referee) for many useful suggestions that led to the improvement of this paper. This work was supported in part by the following grants: AST 92-23967 to EO, and AST 92-17961 to JL.

REFERENCES

Acker A., Koppen J., Stenholm B., Raytchev B., 1991, A&AS, 89, 237
Armandroff T. E., 1989, AJ, 97, 375
Armandroff T. E., DaCosta G. S., Zinn R., 1991, AJ, 104, 164
Arnett W. D., 1978, ApJ, 219, 1008
Arp H. C., 1955, AJ, 60, 317
Arp H. C., 1965, ApJ, 141, 43
Baade W., 1951, Publ. Obs. Univ. Michigan, 10, 7
Balcells M., Peletier R. F., 1994, AJ, 107, 135
Barbuy B., Grenon M., 1990, in Jarvis B., Terndrup D., eds, Bulges of Galaxies. ESO, Garching, p. 47
Bessell M.S., 1986, PASP, 98, 1303
Bica E., Barbuy B., Ortolani S., 1991, ApJ, 382, L15
Binney J., Gehrard O. E., Stark A. A., Bally J., Uchida K. I., 1991, MNRAS, 252, 210
Blanco V., 1965, in Blaauw A., Schmidt M., eds, Vol. 5, Galactic Structure, Stars and Stellar Systems. Univ. Chicago Press, Chicago, p. 241
Blanco V. M., Terndrup D. M., 1989, AJ, 98, 843
Blitz L., Spergel D., 1991, ApJ, 370, 205
Buzzoni A., Fussi Pecci F., Buonanno R., Corsi C., 1983, A&A, 128, 94
Canterna R., 1976, AJ, 81, 228
Carlberg R. G., 1984, ApJ, 286, 403
Carney B. W., Latham D. W., Laird J. B., 1990, AJ, 99, 752
Cook K., 1987, PhD thesis, Steward Observatory, Univ. Arizona
Cudworth K. M., 1986, AJ, 92, 348
Dwek E. et al., 1994, ApJ, in press
Edvarsson B., Andersen J., Gustafsson B., Lambert D. L., Nissen P. E., Tomkin J., 1993, AA, 275, 101
Eggen O. J., Lynden-Bell D., Sandage A., 1962, ApJ, 136, 748
Faber S. M., Friel E. D., Burstein D., Gaskell C. M., 1985, ApJS, 57, 711
Frenk C. S., White S. D. M., 1982, MNRAS, 198, 173
Friedli D., Benz W., Kennicutt R., 1994, ApJ, 430, L105
Friel E. D., 1987, AJ, 93, 1388
Friel E. D., Janes K. A., 1993, A&A, 267, 75
Frogel J. A., 1988, ARA&A, 26, 51
Frogel J. A., Terndrup D. M., Blanco V. M., Whitford A. E., 1990, ApJ, 353, 494
Geisler D., Claria J. J., Minniti D., 1991, AJ, 102, 1836
Geisler D., Friel E. D., 1990, AJ, 104, 128
Gorgas J., Faber S. M., Burstein D., Gonzalez J. J., Courteau S., Prosser C., 1993, ApJS, 86, 153
Greggio L., Renzini A., 1990, ApJ, 364, 35
Hartwick F. D. A., 1976, ApJ, 209, 418
Henry R. B. C., Howards J. W., 1995, ApJ, 438, 170
Hill J. M., Lesser M. P., 1988, in Robinson L. B., ed., Instrumentation for Ground-Based Optical Astronomy: Present and Future. Springer-Verlag, New York, p. 233
Holtzmann J. et al., 1993, AJ, 106, 1826
Horch E., Demarque P., Pinsonneault M., 1992, ApJ, 388, L53
Iben I., 1968, Nat, 220, 143
Ingerson T. E., 1988, in Barden S. C., ed., ASP Conf. Ser. Vol. 3, Fiber Optics in Astronomy. Astron. Soc. Pac., San Francisco, p. 99
Janes K. A., 1978, ApJ, 243, 135
Kent S. M., 1992, ApJ, 387, 181
Kinman T. D., Feast M. W., Lasker B. M., 1988, AJ, 95, 804
Larson R. B., 1976, MNRAS, 176, 31
Lee Y. W., 1992, AJ, 104, 1780
Martin P., Roy J. R., 1994, ApJ, 424, 599
Matteucci F., Brocatto E., 1990, ApJ, 365, 539
McQuitty R. G., Jaffe T. R., Friel E. D., Dalle Ore C. M., 1994, AJ, 107, 539
McWilliam A., Rich R. M., 1994, ApJS, 91, 749
Minniti D., 1993, PhD thesis, Steward Observatory, Univ. Arizona
Minniti D., 1995a, A&A, in press
Minniti D., 1995b, A&A, in press
Minniti D., 1995c, ApJ, in press
Minniti D., 1995d, AJ, 109, 1663
Minniti D., Coyne G. V., Claria J. J., 1992, AJ, 103, 871
Minniti D., Olszewski E., Rieke M., 1995, AJ, in press
Minniti D., White S. D. M., Olszewski E., Hill J. H., 1992, ApJ, 393, L47
Morgan W. W., Mayall N. U., 1957, PASP, 69, 291
Morrison H. L., Harding P., 1993, in Habing H., DeJonghe H., eds, IAU Symp. 153, Galactic Bulges. Kluwer, Dordrecht, p. 297
Morrison H. L., Harding P., 1993, PASP, 105, 977
Nassau T., Blanco V. M., 1958, ApJ, 128, 46
Nomoto K., Thielemann F., Yokoi Y., 1984, ApJ, 286, 644
Norris J. E., Bessell M. S., Pickles A. J., 1985, ApJS, 58, 463
Pagel B., Edmunds M. G., 1981, ARA&A, 19, 77
Pfenniger D., Norman C., 1990, ApJ, 363, 391
Pier J. R., 1983, ApJS, 53, 791
Ratag M. A., Pottasch S. R., Dennerfeld M., Menzies J. W., 1992, A&A, 255, 255

Renzini A., 1992, in Barbuy B., Renzini A., eds, IAU Symp. 149 The Stellar Populations of Galaxies. Kluwer, Dordrecht, p. 325
Renzini A., 1993, in Habing H., DeJonghe H., eds, IAU Symp. 153 Galactic Bulges. Kluwer, Dordrecht, p. 151
Renzini A., 1994, A&A, 285, L5
Rich R. M., 1988, AJ, 95, 828
Rich R. M., 1993a, in Habing H., DeJonghe H., eds, IAU Symp. 153 Galactic Bulges. Kluwer, Dordrecht, p. 169
Rich R. M., 1993b, in Majewski S. R., ed., ASP Conf. Series Vol. 49, Galaxy Evolution: The Milky Way Perspective. Astron. Soc. Pac., San Francisco, p. 65
Schmidt G. D., Weymann R. J., Foltz C. B., 1989, PASP, 101, 712
Searle L., Zinn R., 1978, AJ, 225, 357
Sellwood P. A., 1993, in Habing H., DeJonghe H., eds, Galactic Bulges. Kluwer, Dordrecht, p. 391
Shaver P., McGee R., Newton L. M., Danks A. C., Pottasch S. R., 1983, MNRAS, 204, 53
Sneden C., Kraft R. P., Langer G. E., Prosser C. F., Shetrone M. D., 1994, AJ, 107, 1773
Spite M., Spite F., 1985, ARA&A, 27, 279
Stanek K. Z., Mateo M., Udalski A., Szymanski M., Kaluzny J., Kubiak M., 1994, ApJ, 429, L73
Stasinska G., 1993, in Habing H., DeJonghe H., eds, IAU Symp. 153 Galactic Bulges. Kluwer, Dordrecht, p. 117
Stasinska G., Tylenda R., Acker A., Stenholm B., 1991, A&A, 247, 173
Stetson P. B., 1987, PASP, 99, 191
Suntzeff N. B., Mateo M., Terndrup D., Olszewski E. W., Geisler D., Weller W., 1993, ApJ, 418, 208
Terndrup D. M., 1988, AJ, 96, 884
Terndrup D. M., 1993, in Habing H., DeJonghe H., eds, IAU Symp. 153 Galactic Bulges. Kluwer, Dordrecht, p. 87
Terndrup D. M., Blanco V. M., Frogel J. A., Whitford A. E., 1990, ApJ, 353, 494
Terndrup D. M., Frogel J. A., Whitford A. E., 1990, ApJ, 357, 453
Terndrup D. M., Frogel J. A., Whitford A. E., 1991, ApJ, 378, 742
Thielemann F.-K., Hashimoto M., Nomoto K., 1990, ApJ, 349, 222
Toomre A., 1977, in Tinsley B. M., Larson R. B., eds, The Evolution of Galaxies and Their Stellar Populations. Yale Univ. Press, New Haven, p. 401
Twarog B., Anthony-Twarog B., 1994, AJ, 107, 1371
Tyson N. D., 1991, PhD thesis, Univ. Columbia
Tyson N. D., 1992, in Holt S. S., Verter F., eds, AIP Conf. Proc. 278, Back to the Galaxy. Am. Inst. Phys., New York, p. 141
Tyson N. D., Rich R. M., 1993, in Habing H., DeJonghe H., eds, IAU Symp. 153 Galactic Bulges. Kluwer, Dordrecht, p. 333
Udalski A., Szymanski M., Kaluzny J., Kubiak M., Mateo M., 1993, Acta Astron., 43, 69
van den Bergh S., 1971, AJ, 76, 1082
Walker A., Terndrup D. M., 1991, ApJ, 378, 119
Wheeler J. C., Sneden C., Truran J. W., 1989, ARA&A, 27, 279
White S. D. M., 1980, MNRAS, 191, 1P
Whitelock P., Menzies J., Feast M., Marang F., Carter B., Roberts G., Catchpole R., Chapman J., 1994, MNRAS, 267, 711
Whitford A. E., 1978, ApJ, 226, 777
Whitford A. E., 1985, PASP, 97, 205
Wyse R. F. G., Gilmore G., 1992, AJ, 104, 144
Wyse R. F. G., Gilmore G., 1993, in Brodie J., Smith G., eds, The Globular Cluster–Galaxy Connection. Astron. Soc. Pac., San Francisco, p. 727
Zaritsky D., Kennicutt R. C., Huchra J. P., 1994, ApJ, 420, 87
Zinn R., 1985, ApJ, 293, 424